

NO_x Modelling of a Complete Diesel Engine/SCR System

Claes Ericson

Division of Combustion Engines
Department of Energy Sciences
Lund University

Licentiate Thesis



LUND INSTITUTE OF TECHNOLOGY
Lund University

© Claes Ericson, All rights reserved
ISRN LUTMDN/TMHP--07/7047--SE
ISSN 0282-1990

Printed in Sweden by Media-Tryck, Lund Februari 2007
Lund 2007

List of papers

Paper I

Transient emission predictions with quasi stationary models

C. Ericson, B. Westerberg and R. Egnell

SAE Technical papers 2005-01-3852, 2005.

Paper II

Modelling diesel engine combustion and NO_x formation for model based control and simulation of engine and exhaust aftertreatment system

C. Ericson, M. Andersson, R. Egnell and B. Westerberg

SAE Technical papers 2006-01-0687, 2006.

Paper III

A state-space simplified SCR catalyst model for real time applications

C. Ericson, I. Odenbrand and B. Westerberg

To be submitted to SAE 2007 Powertrain and Fluid Systems.

Abstract

The use of aftertreatment systems and Selective Catalytic Reduction (SCR) in particular, is becoming increasingly more popular as a cost effective way of reducing emissions from heavy duty vehicles. In order to make efficient use of these systems, it is important to have a complete system approach when it comes to calibration of the engine and aftertreatment system. One novel approach to reach the best compromise between low emissions and fuel/urea consumption is to use model based optimization.

To perform model based optimization, extremely computationally efficient, yet accurate models of the engine and aftertreatment system are needed. This is the focus of this thesis; to develop efficient models of primarily NO_x formation in the diesel engine and NO_x reduction using SCR.

The first step involved developing quasi steady emission prediction methods. A physically based correction method termed the Delay Model is presented. Using this compensation method, transient correction factors can be calculated to predict carbon monoxide and particulate emissions from Euro III class diesel engines with reasonable accuracy. On the engines studied, no correction factor is applied for NO_x emissions. The models lack in accuracy to be used for simulation / optimization purposes however.

Improved accuracy of engine-out NO_x predictions was achieved by developing a zero dimensional combustion and NO_x formation model. The model uses a two zone concept and is predictive, i.e. the heat release rate is predicted using fuel injection parameters. NO_x formation is calculated according to the original Zeldovich mechanism. Tabulated data is used to calculate equilibrium concentrations and correction for incomplete combustion. The average calculation time is 50 ms per cycle.

In addition to the engine-out NO_x model, a gas exchange model of the quasi steady filling and emptying type is presented. The modelled engine includes an EGR system and a variable geometry turbocharger (VGT). The model requires a 10ms time step length to remain stable in all conditions, but is extremely fast due to an efficient Simulink implementation.

The SCR catalyst model is based on a state space concept. The catalyst is discretized into six continually stirred tanks in the axial direction, and two wall layers are used to describe the mass transfer in the channel wall. At low temperatures the model uses an implicit method of calculating the coverage differential. At higher temperatures, the model is simplified to a first order system. These simple, yet robust methods allow for long step lengths in the process of solving the differential equations. Using a 0.5 s time step, the computational performance is close to 100 times real time.

The models can be combined to a complete diesel engine and SCR system model. The engine-out NO_x model and the SCR catalyst model have been integrated with excellent results. The integration with the gas exchange model needs more work in order to make the complete model entirely predictive.

The complete model can be used to study the effects of varying EGR rate, injection pressure, injection timing and urea injection on NO_x formation and overall fuel/urea consumption.

Acknowledgements

This work would have been impossible without the help and cooperation of a large number of people:

First, my main supervisor Rolf Egnell, Lund University has offered great support and enthusiasm throughout the work. Björn Westerberg, my supervisor at Scania and Ingemar Odenbrand, my second supervisor at Lund University have taught me everything I know about the mysterious world of catalysts and have always found time to contribute with feedback and interesting ideas during the work.

Special thanks to Magnus Andersson, previously at Lund Institute of Technology, now a colleague at Scania, for his contribution to my second paper and many inspiring discussions.

I would also like to acknowledge all the people at Scania Engine development for always patiently answering my questions and excellent support with the measurements, especially Olof Erlandsson, Ola Stenlåås, Jesper Ritzén, Mikael Persson, Martin Nilsson and all the people at the predevelopment section.

This work was partly financed by the Emission Research Programme (EMFO), which the author is greatly thankful for. EMFO is supported by the Swedish Road Administration, the Swedish Environmental Protection Agency and the Swedish Energy Agency.

Last, but not least, I'm grateful for the support and encouragement from my family and wonderful girlfriend Marie-Louise.

Notation and acronyms

A	[m ²]	Current cylinder wall area
A_{egr}	[m ²]	EGR valve active flow area
$A_{exh.sys}$	[m ²]	Inner/outer wall area of exhaust system
A_k	[m ²]	Mass / heat transfer area, catalyst channel segment k
A_s	[m ²]	Catalyst wall cross sectional area
B	[m]	Cylinder bore
C_{HR}	[1/s]	Heat release factor
c_i	[mol/m ³]	Concentration of species i
$c_{i,eq}$	[mol/m ³]	Equilibrium concentration of species i
CO_{corr}	[1]	QS CO correction factor
$c_{P,i}$	[J/kg K] / [J/mol K]	Specific heat capacity of component i
C_{rad}	[J/s K]	Parameter in radiative heat transfer expression
C_{wo}	[1]	Constant in Woschni convective heat transfer expression
d	[m]	Catalyst channel width
$D_{eff,i}$	[m ² /s]	Effective diffusivity, specie i
$d_{exh.sys}$	[m]	Diameter of the exhaust system
D_i	[m ² /s]	Diffusivity, specie i
$D_{K,i}$	[m ² /s]	Knudsen diffusivity, specie i
d_p	[m]	Catalyst mean pore diameter
$E_{A,i}$	[J/mol]	Activation energy, reaction i
f_D	[1]	Catalyst porosity-tortuosity factor
f_{eq}	[K]	Temperature dissociation compensation
f_{exh}	[1/s]	Exhaust manifold temperature look-up table
$f_{exhcorr}$	[1]	Black box exhaust temperature correction factor
f_{ID}	[deg]	Ignition delay
F_{tot}	[mol/s]	Total molar flow
F_v	[1]	Gray body view factor
h_c	[J/s m ² K]	In-cylinder convective heat transfer coefficient
h_{cve}	[J/s m ² K]	External convective heat transfer coefficient
h_{cvi}	[J/s m ² K]	Internal convective heat transfer coefficient
h_{gi}	[J/s m ² K]	Generalized internal heat transfer coefficient
h_k	[J/s m ² K]	Catalyst heat transfer coefficient, segment K
$H_{v,i}$	[J/mol]	Heat of vaporization, specie i
J_{trb}	[Nm/s ²]	Turbocharger inertia
k_c	[m/s]	Catalyst film mass transfer coefficient
k_{es}	[s ² /m ⁴]	Restriction constant, exhaust system
k_i	[m ³ /s]/[m ³ /s kg cat] /[mol/s kg cat]	Pre exponential factor / rate coefficient, reaction i
M	[Nm]	Torque
m_{burn}	[kg]	Burned zone mass
$m_{exh.sys}$	[kg]	Mass of the exhaust system
m_{flame}	[kg]	Mass of freshly burned mass element (flame)
M_i	[kg]	Molar mass of specie i
$m_{s,k}$	[kg]	Total mass solid material, catalyst channel segment k
M_{trb}, M_{cmp}	[kg/s]	Turbine / compressor torque
N_C	[mol/kg]	Specific number of active sites of catalyst
n_{eng}	[rpm]	Engine speed
n_{trb}, n_{cmp}	[rpm]	Turbine/compressor speed
Nu	[1]	Nusselt number
p	[bar]	Cylinder pressure
p_{amb}	[bar]	Ambient pressure
p_{es}	[bar]	Exhaust system pressure
p_{evo}	[bar]	Pressure at exhaust valve opening
p_{im}, p_{em}	[bar]	Intake / exhaust manifold pressure
p_{max}	[bar]	Peak cylinder pressure
p_{rail}	[bar]	Common rail pressure
$Q_{fuel,inj}$	[J]	Injected fuel energy
Q_g, Q_n	[J]	Gross / Net heat released

$Q_{ht,conv}$	[J]	Combustion convective heat loss
$Q_{ht,rad}$	[J]	Combustion radiative heat loss
q_k	[J/s m ²]	Solid catalyst heat flux
Q_{LHV}	[J]	Lower heating value
R	[J/kg K] / [J/mol K]	General / molar gas constant
Re	[1]	Reynolds number
r_i	[mol/s] / [mol/s kg cat]	Reaction rate, reaction i
Sh	[1]	Sherwood number
t	[s]	Time
T	[K]	Cylinder gas temperature
T_{amb}	[K]	Ambient temperature
T_{atrb}	[K]	Temperature after turbine
T_{burn}	[K]	Burned zone temperature after dissociation compensation
$T_{burn,perf}$	[K]	Burned zone temperature before dissociation compensation
$T_{cat,in}$	[K]	Temperature before catalyst (with urea inj. compensation)
T_{egr}	[K]	EGR temperature
T_{es}	[K]	Exhaust system temperature
T_{evo}	[K]	Exhaust temperature at exhaust valve opening
T_{exh}	[K]	Exhaust temperature before catalyst
T_{exp}	[K]	Expanded burned zone temp
T_{flame}	[K]	Combustion flame temperature
$T_{flame,ad}$	[K]	Adiabatic flame temperature
$T_{flame,ht}$	[K]	Radiation compensated adiabatic flame temperature
T_g	[K]	Gas bulk temperature
T_{im}, T_{em}	[K]	Intake / exhaust manifold temperature
T_{precat}	[K]	Exhaust temperature pre catalyst
T_{ref}	[K]	Reference temperature, diffusion calculations
T_s	[K]	Catalyst surface temperature
T_w	[K]	Exhaust system wall temperature
T_{wall}	[K]	Combustion chamber wall temperature
u	[m/s]	Average in-cylinder gas velocity
u_{egr}	[V]	EGR valve actuator control signal
u_{vgt}	[V]	VGT actuator control signal
V	[m ³]	Current cylinder volume
V_{em}/V_{im}	[m ³]	Volume of exhaust / inlet manifold
$\nu_{i,j}$	[1]	Stoichiometric factor, specie i in reaction j
W_{air}	[kg/s]	Air mass flow
W_{egr}	[kg/s]	EGR mass flow
$W_{eng,in}$	[kg/s]	Engine in mass flow
$W_{eng,out}$	[kg/s]	Engine-out mass flow
W_{es}	[kg/s]	Exhaust system mass flow
W_{fuel}	[kg/s]	Fuel mass flow
$w_{k,n}$	[kg]	Catalyst mass, segment k, layer n
W_{trb}, W_{cmp}	[kg/s]	Turbine / compressor mass flow
W_{urea}	[kg/s]	Urea mass flow
x	[%]	Conversion
x_{egr}	[%]	EGR rate
x_{H2O}	[%]	Molar ratio water to urea
y_i	[1]	Molar fraction, specie i
θ	[deg]	Crank angle degree
δ	[kg/stroke]	Injected fuel mass
τ	[s]	Characteristic time constant, first order method calculations (catalyst model)
ε	[1]	Emissivity
σ	[W/m ² K ⁴]	Stefan-Boltzmann constant
λ, λ_{local}	[1]	Global / local air fuel equivalence ratio
$\lambda_{dyn/QS}$	[1]	Dynamic / Quasi Stationary global air-fuel equivalence ratio
ΔH_j	[J/mol]	Heat of reaction j
λ_i	[W/m K]	Heat conductivity, component i
γ_i	[1]	Specific heat value ratio of specie i

β_i	[1]	Coefficient for implicit method calculations (catalyst model)
α_i	[1]	Coefficient for first order method calculations (catalyst model)
$\Gamma_{i,k,n}$	[m ³ /s]	Mass transfer coefficient, specie i in catalyst layer n, segment k
τ_{lag}	[s]	Turbocharger delay time
θ_{NH3}	[1]	Catalyst ammonia coverage
α_{SOC}	[deg]	Start of combustion
α_{SODC}	[deg]	Start of diffusion combustion
α_{SOI}	[deg]	Start of injection
θ_{ss}	[1]	Steady state catalyst ammonia coverage
Δt	[s]	Time step length
$\omega_{trb}, \omega_{cmp}$	[rad/s]	Turbine/compressor angular speed
η_{trb}, η_{cmp}	[rpm]	Turbine/compressor efficiency
Δx_n	[m]	Wall thickness of catalyst layer n
Δz_k	[m]	Length of catalyst segment k
EGR	Exhaust Gas Recirculation	
EICO/EIPM	Emission Index CO/PM	
ETC	European Transient Test Cycle	
ESC	European Stationary Test Cycle	
QS	Quasi Stationary	
SCR	Selective Catalytic Reduction	
TEOM	Tapered Element Oscillating Microbalance	
TNO	The Netherlands Organization for Applied Scientific Research	
VGT	Variable Geometry Turbine	

Table of content

1	INTRODUCTION.....	1
1.1	BACKGROUND.....	1
1.2	SELECTIVE CATALYTIC REDUCTION	2
1.3	THE OPTIMIZATION PROBLEM.....	3
1.4	OBJECTIVE	4
1.5	METHOD	4
2	QUASI STATIONARY ENGINE-OUT EMISSION MODELS	5
2.1	INTRODUCTION	5
2.2	APPLICATION TO EURO III ENGINES	5
2.3	TRANSIENT CORRECTION	6
2.3.1	<i>The Delay Model</i>	7
2.4	RESULTS	10
3	ENGINE-OUT NO_x MODEL.....	13
3.1	PREDICTIVE HEAT RELEASE MODEL.....	14
3.2	BURNED ZONE / NO FORMATION MODEL.....	17
3.3	RESULTS	20
4	GAS EXCHANGE MODEL	24
4.1	THE MODEL	24
4.1.1	<i>Compressor</i>	24
4.1.2	<i>Intake and exhaust manifold</i>	25
4.1.3	<i>EGR system</i>	25
4.1.4	<i>Turbine</i>	26
4.1.5	<i>Exhaust system</i>	26
4.1.6	<i>Exhaust temperature</i>	26
4.2	RESULTS	27
5	COMPLETE ENGINE MODEL.....	28
5.1	MODEL STRUCTURE	28
5.2	RESULTS	29
6	SCR CATALYST MODEL.....	31
6.1	REACTIONS	31
6.2	MASS AND HEAT BALANCES.....	32
6.3	UREA DECOMPOSITION BEFORE THE CATALYST	36
6.4	RESULTS	37
7	COMBINED ENGINE AND SCR CATALYST MODEL.....	40
7.1	MODEL STRUCTURE	40
7.2	RESULTS	40
8	SUMMARY	43
9	FUTURE WORK.....	44
10	REFERENCES.....	45
11	SUMMARY OF PAPERS	46

1 Introduction

1.1 Background

Two decades ago, emissions legislation for heavy trucks and buses were not very challenging for the manufacturers. The primary focuses were fuel efficiency and durability. This picture has changed substantially though with ever increasing demands for low emissions from both European and American authorities. In the 90's, Euro III emissions were achieved using higher injection pressure for low particulate emissions and retarded injection for lower NO_x emissions. Euro IV emissions however, proved difficult to achieve using traditional technology. Some manufacturers introduced cooled EGR to decrease NO_x, others used Selective Catalytic Reduction (SCR) using urea / AdBlue as reduction agent. Using SCR, the injection timing can be advanced which gives favourable fuel economy. Engines achieving Euro V emission levels have also been demonstrated using either EGR or SCR technology. The Euro VI standard is yet to be determined; possibly it will be harmonized with the American EPA 10 legislation. Such low NO_x levels (<0.3 g/kWh) will require even more advanced engine technology and more optimization work. Hydrocarbon (HC) and carbon monoxide (CO) are also regulated, although these emission levels are generally not difficult to achieve in diesel engines due to the high air-fuel ratio.

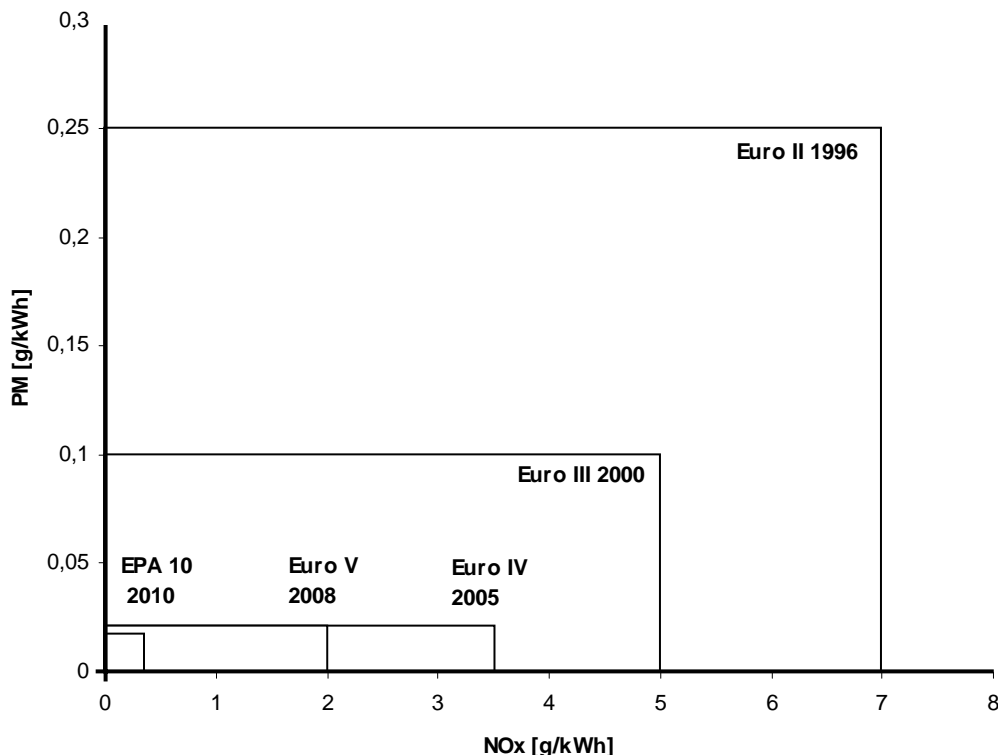


Figure 1 Historical view of emission legislation for heavy truck and bus engines.

CO₂ emissions are currently not regulated by legislation. In the near future it is likely that such legislation will come into effect, or possibly taxation which will increase the demand for fuel efficient engines with correspondingly low CO₂ emissions.

Fuel efficiency has always been an important factor for heavy truck customers; despite this the current engines have poorer efficiency than a decade ago because of the stringent NO_x/PM legislation. The trade-off between low emissions and fuel efficiency will be an even more important challenge in the close future for diesel engine developers.

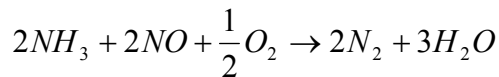
1.2 Selective catalytic reduction

Selective catalytic reduction (SCR) of NO_x using ammonia, NH₃ or urea, CO(NH₂)₂ as a reduction agent has been around since the 1970's in power plants and other stationary applications. In the 1990's SCR systems for mobile applications were developed, at first for marine applications and in 2004 the first commercially available heavy truck with a urea-SCR system was available. Urea is typically the preferred reduction agent in mobile applications because of its odour-free non-poisonous properties. Urea is sold commercially under the name AdBlue as an aqueous solution consisting of 32.5 % urea.

A urea-SCR system consists of three major building blocks:

1. Urea dosing system
2. Control system
3. SCR catalyst

The urea is injected into the exhaust stream from the urea dosing system. The injection point should preferably be some distance before the catalyst to ensure proper mixing. The urea is decomposed (thermolized) to ammonia and isocyanic acid. The isocyanic acid is further hydrolyzed to ammonia and carbon monoxide. The ammonia reacts on the catalyst surface with NO according to:



The result after the reduction is nitrogen and water only. Unfortunately, it is not possible to reach 100 % NO_x reduction, especially not during transient conditions. One of the key factors for achieving high conversion is temperature. The SCR catalyst has a temperature window with a lower limit of approximately 200°C and a higher limit of around 450-500°C. Outside this window, the reduction capability of the catalyst is severely decreased. The catalyst also has much slower dynamics compared to the engine; the catalyst typically requires several minutes before reaching chemical equilibrium compared to a few milliseconds for the diesel engine. It is also important to have proper control of the urea dosing to avoid ammonia slip, i.e. ammonia in the exhaust gas after the catalyst. Ammonia has a distinct unpleasant smell and is also regulated by legislation.

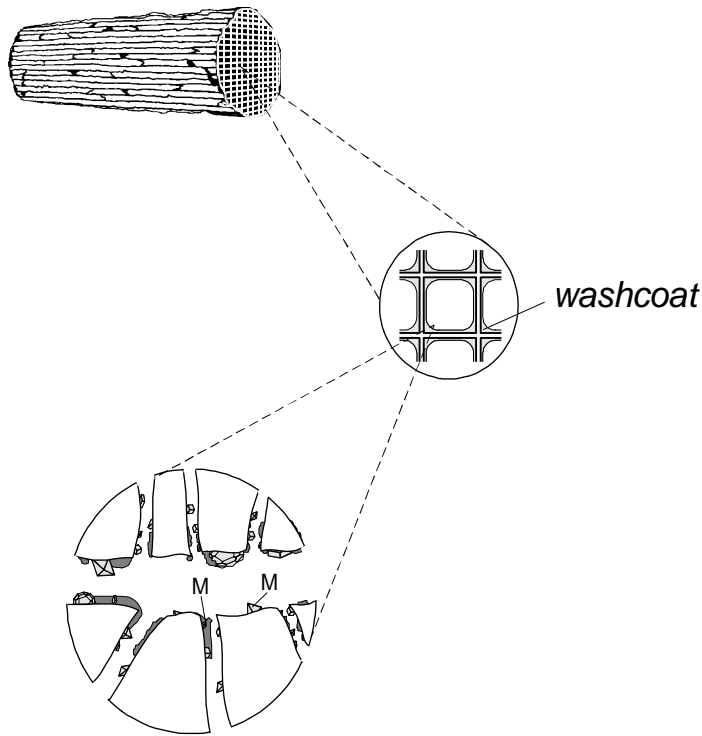


Figure 2 Illustration of a typical monolith catalyst and its porous structure.

The dominating catalyst structure used in automotive applications is the monolith, illustrated in Figure 2. The monolith catalyst achieves high surface area and yet a low pressure drop. Two types of monolith catalysts are commercially available. The first type is built on an inert structure, generally consisting of cordierite, $2\text{MgO}\cdot 2\text{Al}_2\text{O}_3\cdot 5\text{SiO}_2$. The inert structure is coated with a porous material (the washcoat) which further increases the surface area. The most common washcoat material in SCR catalysts is Titanium dioxide, TiO_2 . The washcoat is coated with the catalytically active elements. In the second type of monolith catalysts, the entire catalyst structure incorporates the catalytic material, i.e. no inert material is used. Different additives such as silica are used to create the monolith structure. Common active ingredients in automotive SCR catalysts are vanadium pentoxide, V_2O_5 mixed with tungsten trioxide, WO_3 .

1.3 The optimization problem

To achieve emission levels corresponding to Euro V or beyond while maintaining good fuel economy, it is important that the engine and its aftertreatment system is optimized using a complete system approach. This is not a trivial task though because of the large number of variables which control emissions and fuel consumption in the complex diesel engines of today. Assuming that the engine incorporates a common rail fuel injection system, an EGR system aided by a Variable Geometry Turbocharger (VGT) and a urea SCR system, the following parameters must be optimized in each operating point:

- Injection timing
- Number of injections
- Separation between injections
- Injected fuel amount in each injection
- Injection pressure
- EGR valve position

- VGT actuator position
- Urea dosing

Clearly, this requires substantial time in the engine test bed if all combinations of these variables are to be tested. In addition, because of the slow dynamics of the SCR catalyst, the optimization problem is time dependent making it an extremely complex task. It can be overall cost effective to run the engine at less than optimal settings in some operating conditions to gain advantages during other conditions. Factors such as urea versus diesel fuel costs and driving conditions can also affect the optimal calibration of the complete engine/aftertreatment system.

One novel approach to solve these problems is to use model based optimization and control. The models should preferably be of such simplicity that they can be executed in real time in the engine control system or millions of times in a short time span in the process of offline optimization.

1.4 Objective

This work intends to develop models for engine-out emissions (NO_x primarily) and SCR catalyst models. The models should be of such low complexity that they can be used for optimization and control purposes while maintaining good agreement with measurements.

1.5 Method

The models were developed in Matlab. To validate the models, experiments were performed on diesel engines during both steady state and transient conditions.

2 Quasi stationary engine-out emission models

2.1 Introduction

The most intuitive, and traditional method to predict engine-out emissions is to use quasi stationary calculations (QS). A large number of steady state emission measurements are performed on the engine and emission maps are created, usually using engine speed and torque or injected fuel amount on the x- and y-axis.

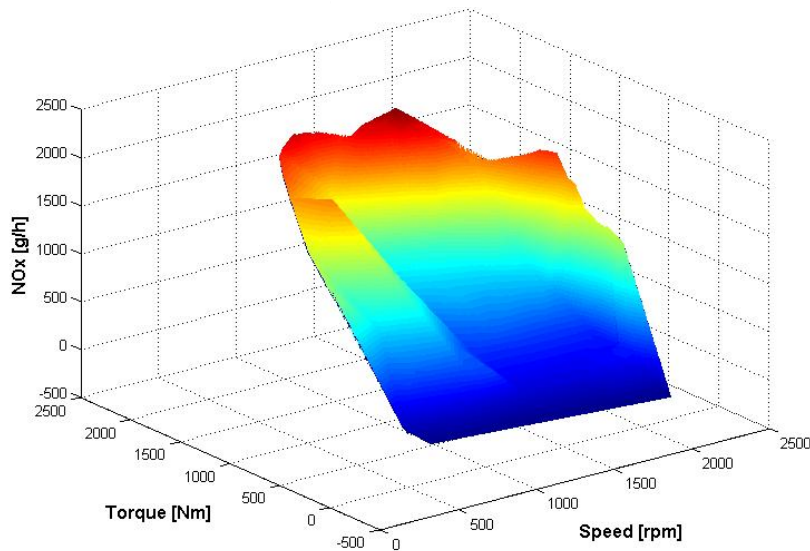


Figure 3 NO_x map of a typical Euro III diesel engine.

Using the engine maps, quasi stationary emissions and fuel consumption during transient test cycles can be calculated. The advantage using engine maps for simulating emissions is the low complexity; all that is needed is a simple interpolation in each time step.

2.2 Application to Euro III engines

Measurements are performed on three 12-litre turbocharged heavy truck engines certified for Euro III, denoted engine A-C. For map generation, a total of approximately 100 steady state points are measured. A total of four transient test cycles, the ETC and the TNO real world driving cycle part 1-3 are run on all engines. The ratios between simulated and measured emissions are shown in Table 1.

Table 1 Accumulated ratio simulated/measured emissions over the four test cycles.

	NO _x	CO	PM	HC
Engine A	0.90	0.61	0.70	1.54
Engine B	1.11	0.36	0.45	1.47
Engine C	0.79	0.52	0.50	1.30

NO_x is reasonably well predicted, although inconsistently over and under estimated for the different engines. Carbon monoxide and particulate emissions are under estimated in all cases, indicating that the emissions are higher during transient operation than the corresponding steady state emissions. Hydrocarbons are over estimated. Because of the substantial deviations, transient correction of the quasi stationary values is needed.

2.3 Transient correction

Transient correction algorithms have previously been suggested by Hausberger et al. [1]. The authors use statistical methods to correct the emissions based on analyzing the transient properties of the test cycle. This results in correction factors for the accumulated emissions, but no time resolved correction. Egnell [2] extends the transient correction to time resolved correction. The work by these two authors has been conducted in the context of estimating emissions from heavy duty vehicle populations in real world applications.

The deviation in NO_x is likely related to different injection timing strategies during transient operation compared to steady state, commonly referred to as “dynamic mapping”. Without detailed knowledge of the engine control system, using only torque and speed as inputs, it’s not possible to make a satisfactory transient correction of the NO_x predictions. Note that dynamic mapping also influences other regulated emissions such as carbon monoxide and particulates. The substantial under estimation of these two emissions is mostly an effect of air shortage / turbo lag as will now be discussed.

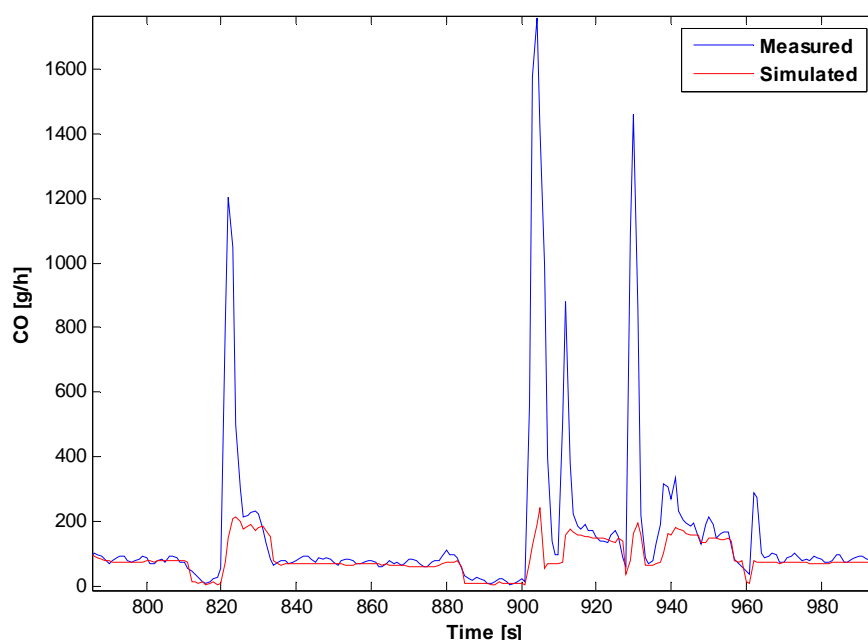


Figure 4 Measured and QS simulated CO, engine B, sequence of the ETC.

Carbon monoxide emissions are satisfactorily estimated during steady sequences of the test cycles. During transients however, there is a distinct under estimation which accounts for the error in the accumulated values. Figure 4 illustrates this phenomenon. As discussed in the previous section, particulate emissions are also under estimated by the quasi stationary calculations. Unfortunately the Tapered Element Oscillating Microbalance (TEOM) instrument used for time resolved particulate measurements

lacks in accuracy and response time, and even registers negative emissions in some cases (Figure 5). The TEOM instrument gives accurate steady state results however, and the accumulated emissions over a test cycle are in agreement with gravimetric measurements. Despite the questionable PM measurements, a similar behaviour as for CO emissions can be noted, the QS predictions are reasonably accurate during steady sequences, and deviate during transients.

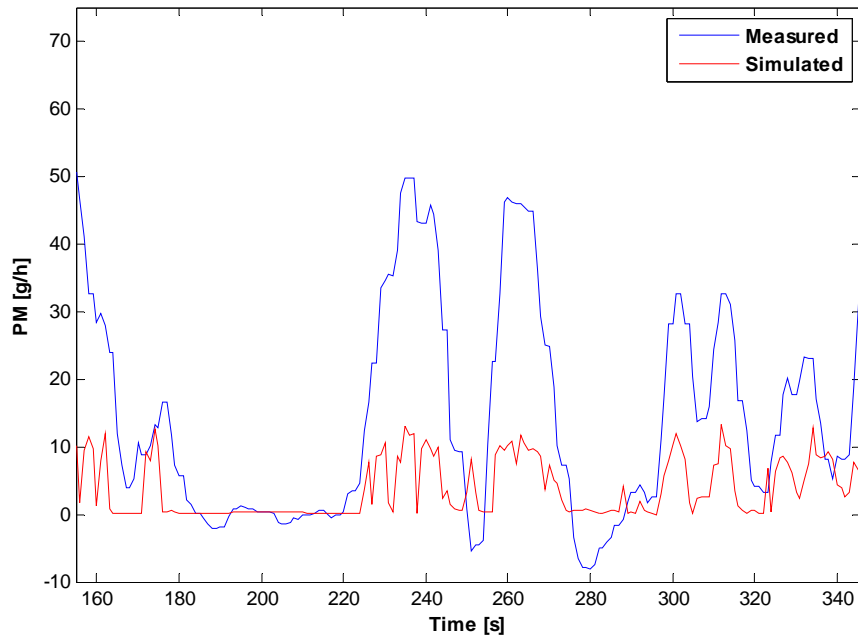


Figure 5 Measured and QS simulated PM, engine B, sequence of the ETC.

2.3.1 The Delay Model

During the onset of a positive load transient the global air-fuel equivalence ratio (λ) value will be lower for a given operating point compared to steady state conditions. The fuel injection system typically has a much faster response time than the turbocharger resulting in a delayed air mass flow compared to the fuel mass flow and thus a lower λ during a positive load transient and a higher λ during a negative transient. The low λ at the beginning of a positive transient will have a substantial effect on emissions. In heavy truck engines the fuel mass flow is restricted to a certain extent by the smoke limiter during transients (to avoid excessive soot), but the effect of turbocharger lag is still evident.

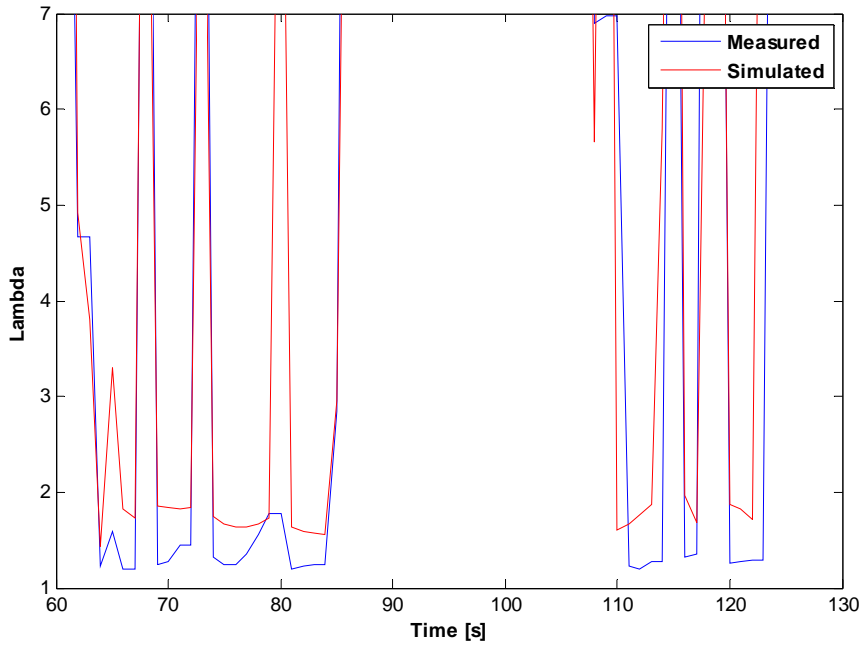


Figure 6 Measured and QS simulated Lambda, engine B, sequence of the ETC.

Measured lambda and the corresponding QS value for a given engine speed and torque are compared in Figure 6 for a highly transient sequence of the ETC. The deviation around 80s is likely related to extrapolation issues with the lambda map.

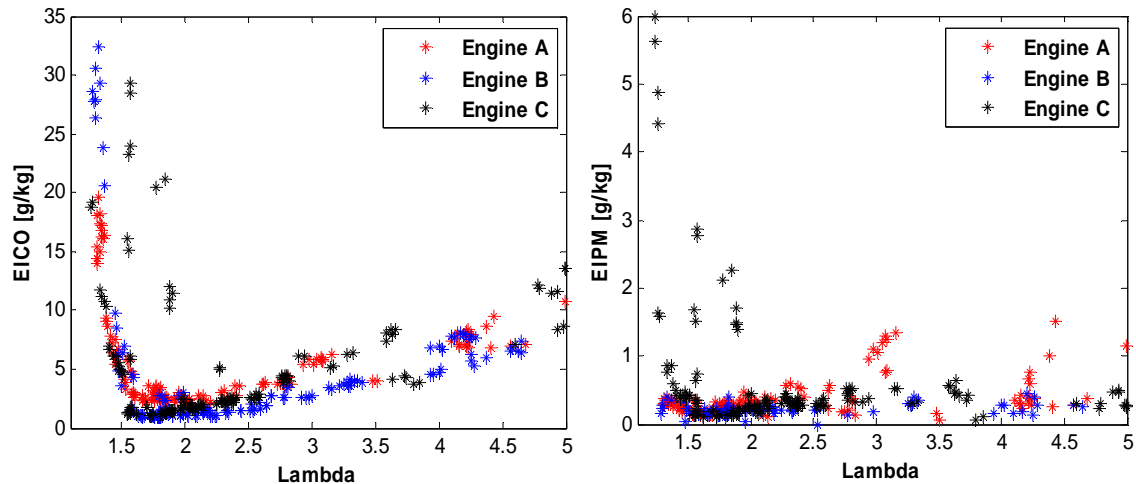


Figure 7 Global lambda dependence of emission index CO and PM.

Figure 7 shows the close correlation between carbon monoxide and particulate emissions to (global) air-fuel equivalence ratio. The increase in PM and CO at higher lambda is likely related to low temperature during the later parts of combustion which results in poor oxidation of the emissions. The interesting part for modelling purposes however, is the sharp knee below approximately lambda 1.7. More CO and PM emissions are produced due to a lower local lambda in the diffusion combustion (rich zones). Despite the high temperature typically associated with the low lambda / high load conditions, the lack of oxygen does not oxidize CO and PM during the expansion. The net result is high CO and PM emissions at low air-fuel equivalence ratios. By fitting polynomial/exponential expressions to the measured emission index versus lambda values, analytical expressions are given which correlates emission

index to global lambda. Jiang et al. use a similar approach correlating CO/PM emissions and lambda [3].

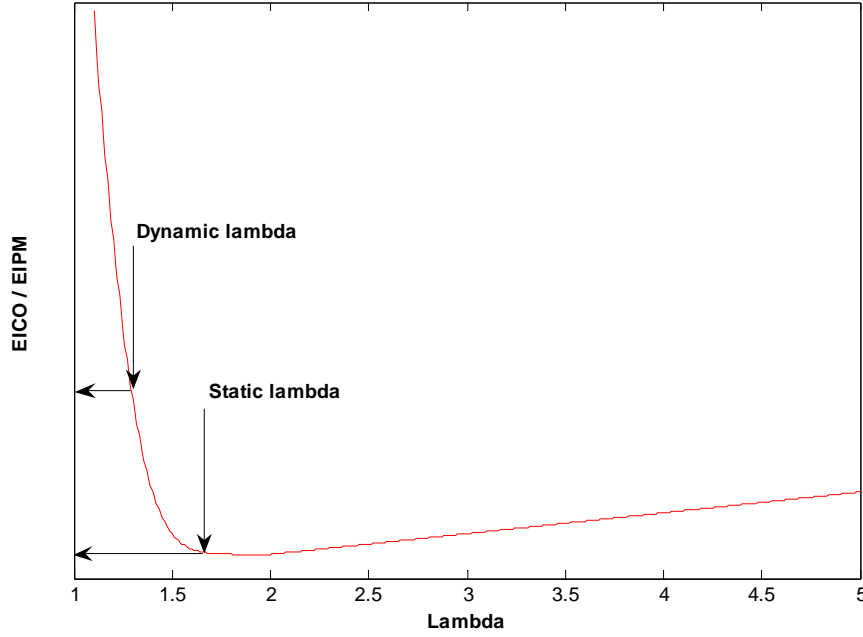


Figure 8 Illustration of the difference between static and dynamic lambda as used in the Delay Model.

The concept behind the Delay Model is to estimate a turbocharger delay time and calculate a corresponding transient/dynamic lambda in each time step. The dynamic lambda will differ (during transients) from the static lambda which is calculated from a lambda map. Using the emission index relations determined from steady state measurements Emission Index Carbon Monoxide/Particulate Matter (EICO/EIPM) values corresponding to the dynamic and static lambdas are calculated (illustrated in Figure 8). In each time step the ratio between these two values is determined. This ratio is multiplied with the emission value determined from the emission map to get the transient corrected emission value.

The delay time is closely related to torque and the torque differential, and is estimated using a simple black box expression:

$$\tau_{lag} = k_1 + k_2 \cdot M + k_3 \cdot \frac{\partial M}{dt} \quad (2.1)$$

The dynamic (corrected) lambda is given by:

$$\lambda_{dyn}(t) = \frac{W_{air}(t - \tau_{lag})}{14.7 \cdot W_{fuel}(t)} \quad (2.2)$$

and finally, the correction factor is the ratio of the emission index values (analogously for particulates):

$$CO_{corr} = \frac{EICO(\lambda_{dyn})}{EICO(\lambda_{QS})} \quad (2.3)$$

A similar correction method was attempted for hydrocarbon emissions (HC) with disappointing results. It is not surprising that transient HC emissions exhibit a

different behaviour than CO and PM; from a reaction mechanism viewpoint, HC is a reactant in the combustion and CO and PM are intermediates / products.

2.4 Results

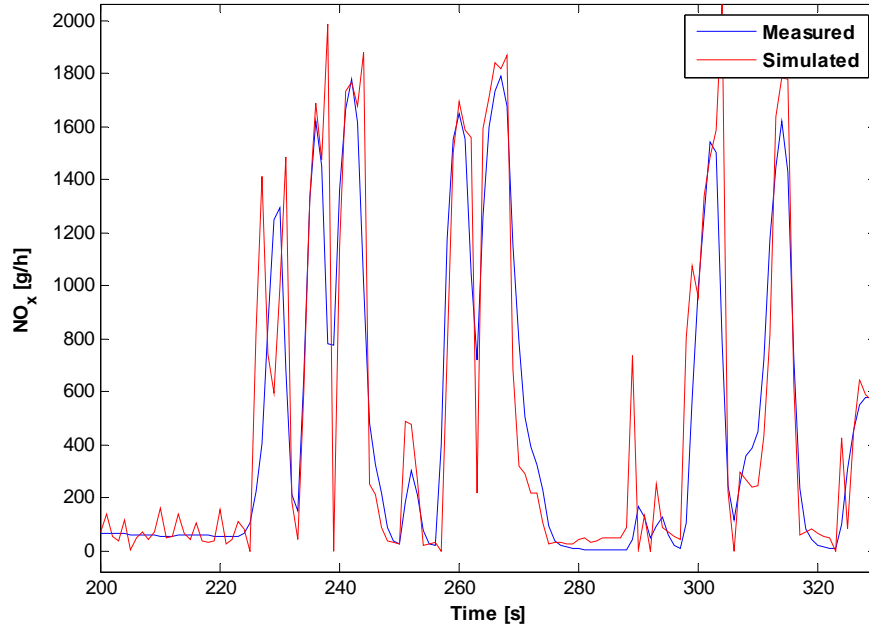


Figure 9 Measured and QS simulated NO_x, Engine A, sequence of the ETC.

NO_x is reasonably well predicted using QS calculations without any compensation. Figure 9 shows measured and simulated quantities during a sequence of the ETC. Measured NO_x concentrations are smoothed because of mixing in the pipes leading to the gas analyzer which will also explain some of the deviations. Note that these simulations are performed on Euro III engines. Dynamic effects of varying EGR rates, injection timing and rail pressure for a given load and speed are not captured with a NO_x model of this type.

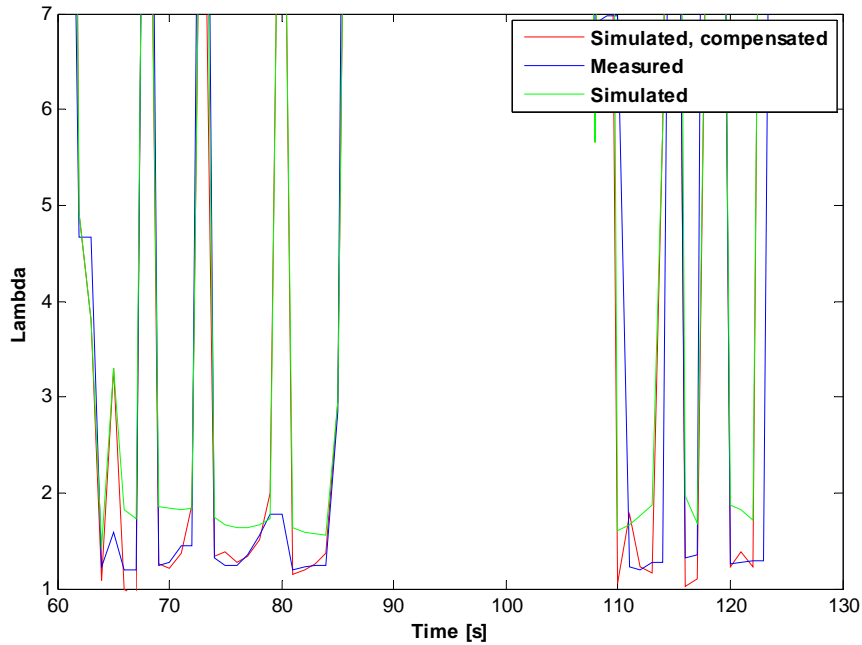


Figure 10 Measured and QS simulated Lambda before and after compensation, Engine B, sequence of the ETC.

The dynamic (compensated) lambda is a better fit to measured values than the static lambda, indicating that the turbo lag delay concept is valid (Figure 10). A plot of time resolved CO emissions shows that the QS values corrected by the Delay Model is in much better agreement with measurements than before compensation (Figure 11). Note however that the Delay Model irregularly under and over compensates. This is related to a less than perfect estimation of the delay time (equation 2.1) and also errors in the curve fit to the emission index versus lambda measurements.

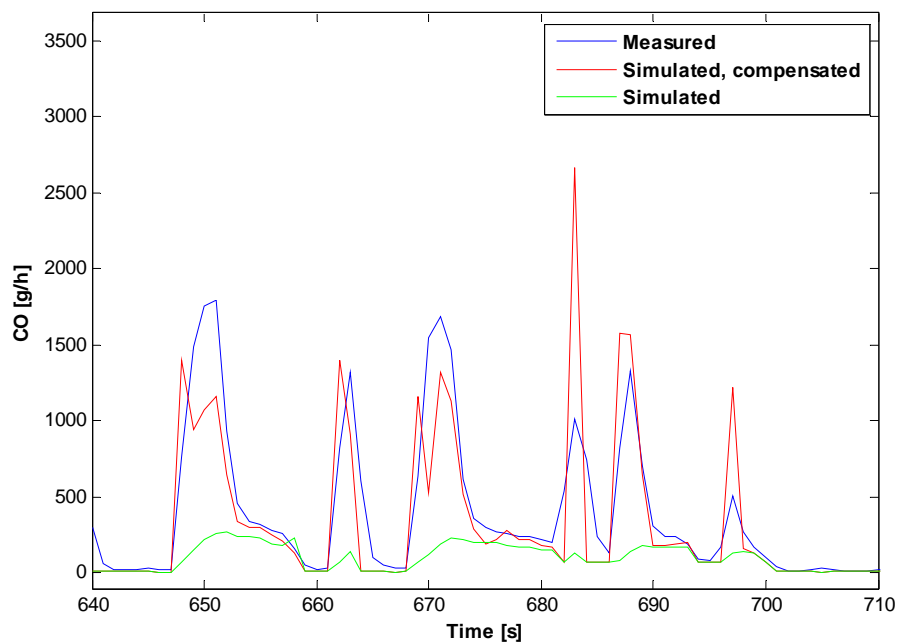


Figure 11 Measured and QS simulated CO before and after transient correction, engine B, sequence of the ETC.

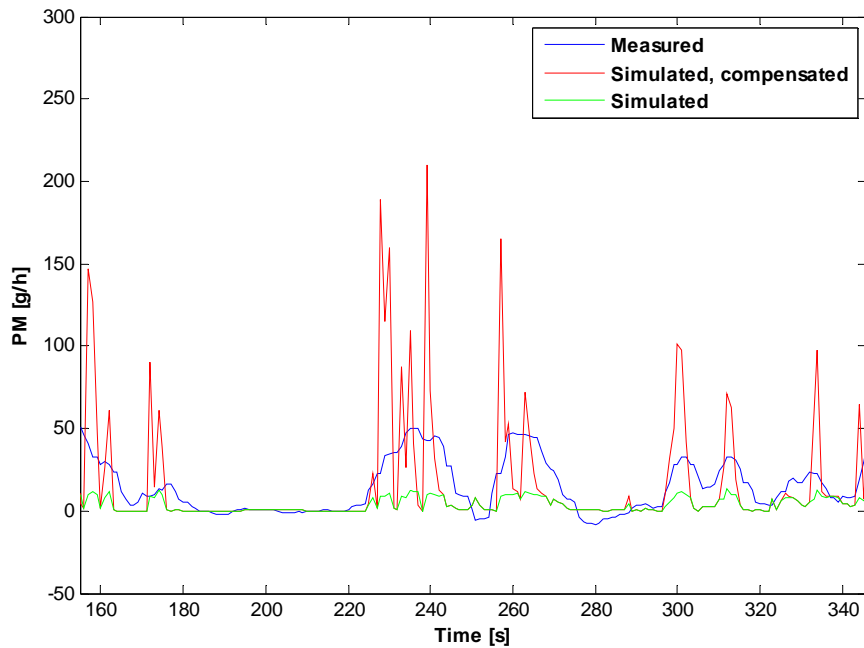


Figure 12 Measured and QS simulated PM before and after transient correction, engine B, sequence of the ETC.

For PM emissions, the slow dynamics of the TEOM instrument makes validation difficult (Figure 12). The transient peaks are roughly in the correct places though, and applying low pass filtering to account for measurement dynamics, good agreement is possible. For both CO and PM emissions, accumulated values over the test cycles show excellent results, the error is less than 2% for engine B. Equally good results can be achieved for the other engines with parameters tuned for the specific engine. Considering the deviations from time resolved measurements, the agreement is not satisfactory enough for engine control and simulation purposes however.

3 Engine-out NO_x model

In this section a more advanced engine-out NO_x model is presented. The model consists of a predictive heat release / combustion model and an NO formation model. The model is based on the zero dimensional model HRNO_x presented by Egnell [4, 5]. Substantial improvements in computational efficiency have been achieved. The modelled engine is an inline six cylinder experimental engine using cooled EGR. The engine is equipped with a variable geometry turbocharger (VGT) and a common rail fuel injection system.

The model is zero dimensional and uses two zones. The combustion chamber contents are divided into one unburned zone which consists of air and EGR, and one burned zone containing the burned results of injected fuel and previous unburned zone contents (Figure 13).

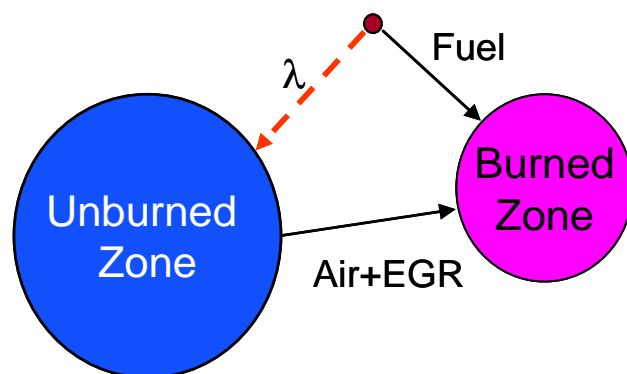


Figure 13 Illustration of the two zone concept.

A number of assumptions analogously with [4] have been made in the modelling process:

- The cylinder content can be described as an ideal gas.
- All combustion takes place at the same local air-fuel equivalence ratio.
- There are no pressure gradients inside the cylinder.
- No air entrainment occurs in the burned zone.
- The zones are compressed isentropically.
- All injected fuel is fully burned.
- Radiative heat losses originate from the flame only.
- NO_x is formed in the burned zone.
- All NO_x content in the recirculated exhaust gas is neglected.
- All released energy originates from injected fuel.

3.1 Predictive heat release model

The heat release model is of the predictive type, i.e. in-cylinder pressure measurements are not needed as inputs.

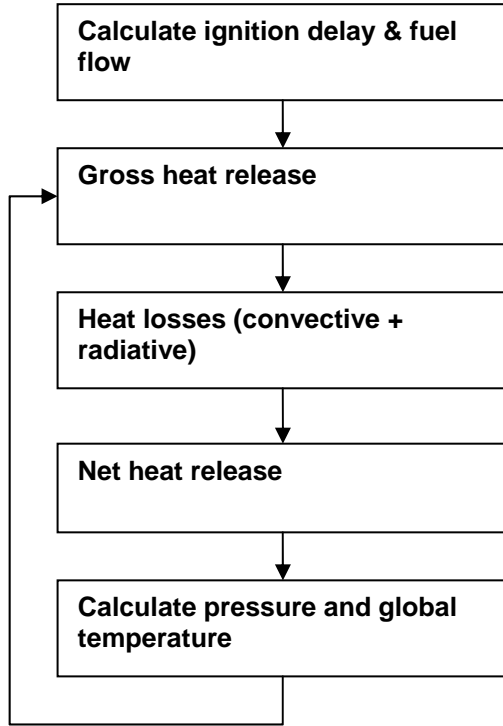


Figure 14 Flowchart of the heat release loop.

A flowchart of the predictive heat release loop is shown in Figure 14. The algorithm will now be described in more detail. First, the ignition delay is estimated using a linear black box model:

$$\alpha_{SOC} - \alpha_{SOI} = f_{ID}(\delta, n_{eng}, p_{rail}, x_{egr}, p_{im}, \lambda) \quad (3.1)$$

δ is the injected fuel mass, n_{eng} the engine speed, p_{rail} the injection system rail pressure, x_{egr} the EGR rate, p_{im} the inlet manifold pressure and λ the air-fuel equivalence ratio. Using the fuel mass flow (W_{fuel}), the injected fuel energy at a crank angle θ is calculated:

$$Q_{fuel, inj} = Q_{LHV} \int_{\alpha_{SOI}}^{\theta} W_{fuel}(\theta) d\theta \quad (3.2)$$

where Q_{LHV} is the lower heating value of the fuel and α_{SOI} the start of injection.

The gross heat release rate is given by:

$$dQ_g = C_{HR} (Q_{fuel, inj} - Q_g), \quad C_{HR} = \begin{cases} 0 & \theta < \alpha_{SOC} \\ C_1 & \alpha_{SOC} \leq \theta < \alpha_{SODC} \\ C_2 & \alpha_{SODC} \leq \theta \end{cases} \quad (3.3)$$

where α_{SOC} and α_{SODC} indicates the start of combustion and start of diffusion combustion. C_1 is an empirically determined constant. C_2 is a second degree polynomial which takes the influence of engine speed on heat release rate during

diffusion combustion into account. The fuel injected during the ignition delay will be added to the injected fuel during a short (fixed) crank angle interval, $\alpha_{SODC}-\alpha_{SOC}$, after the ignition delay. The length of this interval is determined empirically to fit measured heat release rate.

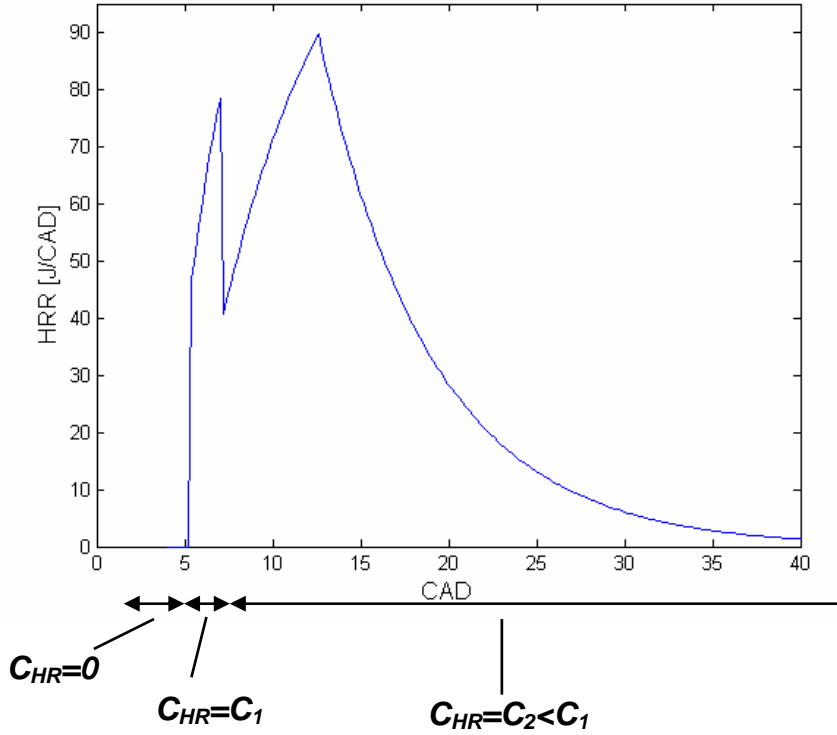


Figure 15 Illustration of the three phases of combustion.

A typical heat release rate curve as given by the model is shown in Figure 15. The figure also illustrates the three phases of diesel combustion (SOI=2 CAD ATDC in this case). Convective heat losses using the cylinder temperature from the previous crank angle step are given by:

$$dQ_{ht,conv}(\theta) = Ah_c(T(\theta - \Delta\theta) - T_{wall}) \quad (3.4)$$

The area A is calculated using the geometric properties of the engine. The gas temperature used is the global in-cylinder gas temperature T (from the previous crank angle step). The wall temperature T_{wall} is fixed at 450 K and h_c is calculated using the Woschni expression [6]:

$$h_c = C_{wo} B^{-0.2} p^{0.8} u^{0.8} T^{-0.55} \quad (3.5)$$

B is the cylinder bore, p the cylinder pressure, u the average gas cylinder velocity and C_{wo} is an empirically determined constant. The flame radiative heat losses are calculated using an approximate flame temperature T_{flame} (from the previous crank angle step):

$$dQ_{ht,rad} = C_{rad}(n_{eng}, \delta) T_{flame}^4 \quad (3.6)$$

where $C_{rad} = c_0 + c_1 \cdot n_{eng} + c_2 \cdot \delta$

The flame temperature is substantially higher than the wall temperature, therefore equation 3.6 is written in a simplified form with T_{wall} omitted. The factor C_{rad} is

calculated by means of a black box expression (a linear regression model) depending on speed and injected fuel mass. C_{rad} is not a strictly physical parameter, it is used in the final step of the combustion model tuning to fit simulated to measured NO_x .

Combining the equations, the net heat release is:

$$dQ_n = dQ_g - dQ_{ht,conv} - dQ_{ht,rad} \quad (3.7)$$

Finally, the pressure is calculated by rearranging the first law of thermodynamics (assuming that the gas composition is constant between two crank angle steps):

$$\frac{dp}{d\theta} = \left(\frac{dQ_n}{d\theta} - \frac{\gamma}{\gamma-1} p \frac{dV}{d\theta} \right) \left(\frac{\gamma-1}{V} \right) \quad (3.8)$$

The global combustion temperature is now given using the ideal gas law.

This sequence of calculations is performed with a fixed crank angle interval. Typically the heat release loop uses a step of 0.1-0.2 CAD in order to capture the rapid changes during the early parts of the combustion cycle.

Exhaust temperature can be estimated fairly accurately using the simulated temperature and pressure at exhaust valve opening, T_{evo} and p_{evo} . A substantial temperature drop will occur from the gas temperature at exhaust valve opening to the exhaust manifold due to the expansion. The expansion will continue over the turbine to close to ambient pressure in the exhaust system. A simple model based on isentropic expansion from the pressure at exhaust valve opening to ambient pressure combined with a black box correction factor is used. The temperature after the turbine is given by:

$$T_{atrb} = f_{exhcorr}(\alpha_{SOI}, \delta, x_{egr}, W_{eng,in}) \left(\frac{p_{amb}}{p_{evo}} \right)^{\frac{\gamma-1}{\gamma}} T_{evo} \quad (3.9)$$

The black box correction factor will correct the values for heat transfer to and from the engine block, exhaust manifold and turbocharger. The exhaust temperature will be further reduced and smoothed before the exhaust gas reaches the silencer / catalyst. This is related to heat transfer to and from the exhaust system. A dynamic mean value exhaust system model is presented by Eriksson [7]. This model is used in the engine model in a simplified form; the heat conduction between engine and exhaust system is neglected. The exhaust system energy balance is given by:

$$\frac{dT_w}{dt} m_{exh.sys} c_{p,exh.sys} = A_{exh.sys} \left(h_{gi} (T_{atrb} - T_w) - h_{cve} (T_w - T_{amb}) - F_v \varepsilon \sigma (T_w^4 - T_{amb}^4) \right) \quad (3.10)$$

where $m_{exh.sys}$, $c_{p,exh.sys}$, $A_{exh.sys}$ are the mass, specific heat and inner/outer surface area (assumed equal) of the exhaust system. T_w is the exhaust system wall temperature. The external convection heat transfer coefficient, h_{cve} and the gray body view factor, F_v as well as the emissivity, ε are assumed to be constant. σ is the Stefan-Boltzmann constant. The generalized internal heat transfer coefficient is given by [7]:

$$h_{gi} = \frac{1 - e^{-\frac{h_{cvi} A_{exh.sys}}{W_{eng,in} c_{p,exh}}}}{h_{cvi} A_{exh.sys}} h_{cvi} \quad (3.11)$$

The internal convective heat transfer coefficient is highly flow dependent, and is estimated using the Nusselt number:

$$h_{cvi} = \frac{Nu\lambda_{exh}}{d_{exh.sys}} \quad (3.12)$$

where the Nusselt number is estimated using the following relation [7]:

$$Nu = 0.48Re^{0.5} \quad (3.13)$$

The pre-silencer / catalyst temperature is given by:

$$T_{precat} = T_w + (T_{atrb} - T_w) e^{\frac{h_{cvi}A_{exh.sys}}{W_{eng,out}c_{p,exh}}} \quad (3.14)$$

The parameters $m_{exh.sys}$, $A_{exh.sys}$, h_{cve} and the lumped parameter $F_v\varepsilon$ are tuned to fit the temperature loss predicted by a GT Power simulation of the studied engine. The temperature sensors used have too poor dynamics to be used for parameter tuning purposes.

3.2 Burned zone / NO formation model

Calculations of burned zone temperature and NO formation are executed in a separate loop. This loop is executed more sparsely than the heat release loop in order to save computational time.

Traditionally, an iteration loop based on the minimization of Gibbs free energy is performed in each crank angle step [4]. The iteration determines the gas composition and the burned zone temperature. This type of model requires too much computational power in order to be used for engine control and transient simulation applications. A simplified method of calculating burned zone temperature in a multi-zone model is presented by Andersson et al. [8, 9]. A variation of this method has been implemented in this two-zone combustion model. Locally stoichiometric combustion is assumed ($\lambda_{local} = 1$) and no air entrainment in the burned zone occurs.

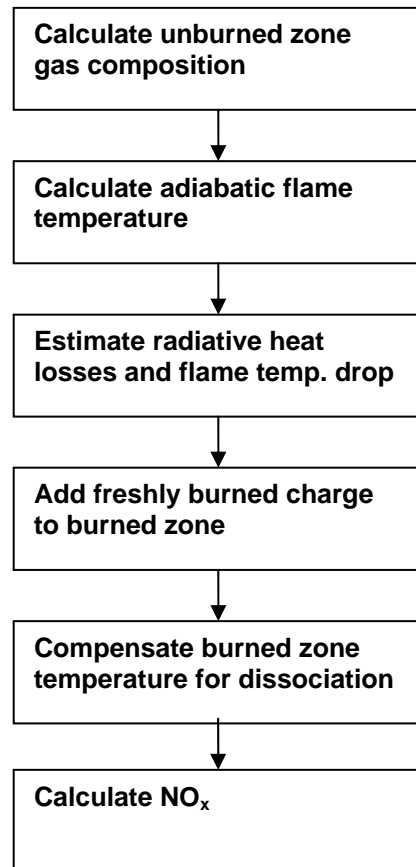


Figure 16 Flow chart of the burned zone / NO formation loop.

The algorithm for updating the burned zone and calculating NO_x formation is presented as a flowchart in Figure 16. First the gas composition of the unburned zone is calculated taking the amount of EGR into account. This will be used to determine the adiabatic flame temperature in the next step (using enthalpy balance between an unburned mass element and a perfectly combusted burned mass element). The enthalpy and specific heats in the iteration are calculated using thermodynamic curve fit coefficients [10]. The burned zone will consist of N₂, CO₂ and H₂O only at all times due to the stoichiometric assumption.

In order to compensate for the incomplete combustion, tabulated data is used. A simplified view is used where the combustion is considered to be perfect and then a table describes the temperature drop which would occur if the combustion products (CO₂, H₂O and N₂) dissociate adiabatically to CO, CO₂, H₂, H, OH, O, O₂, NO, H₂O, N₂ and N. It is a function of pressure, temperature and local air-fuel equivalence ratio. The table is generated using a Gibbs free energy minimization approach analogously to Egnell [4]. Using this table, an estimation of the flame temperature (for radiative heat loss calculations only) is calculated:

$$T_{flame} = T_{flame,ad} - f_{eq}(p, T_{flame,ad}, \lambda_{local}) \quad (3.15)$$

$$dQ_{ht,rad} = C_{rad}(n_{eng}, \delta) T_{flame}^4 \quad (3.16)$$

A new flame temperature which is compensated for radiative heat losses can be calculated according to:

$$T_{flame,ht} = T_{flame,ad} - \frac{dQ_{ht,rad}}{C_{p,exh}} \quad (3.17)$$

Note that the adiabatic flame temperature is never achieved in reality, this is just a number used in the simplified combustion model. The freshly burned mass element is then added to the burned zone. Using the energy balance and assuming that the specific heats are equal, the burned zone temperature is given by:

$$T_{burn,perf}(\theta) = \frac{T_{exp} m_{burn}(\theta - \Delta\theta) + T_{flame,ht} m_{flame}(\theta)}{m_{burn}(\theta)} \quad (3.18)$$

where T_{exp} is the isentropically expanded temperature from the previous crank angle step. m_{burn} denotes the mass in the burned zone and $m_{flame} = m_{burn}(\theta) - m_{burn}(\theta - \Delta\theta)$ is the mass of the freshly burned element (flame).

Next, the burned zone temperature is compensated for incomplete combustion:

$$T_{burn} = T_{burn,perf} - f_{eq}(p, T_{burn,perf}, \lambda_{local}) \quad (3.19)$$

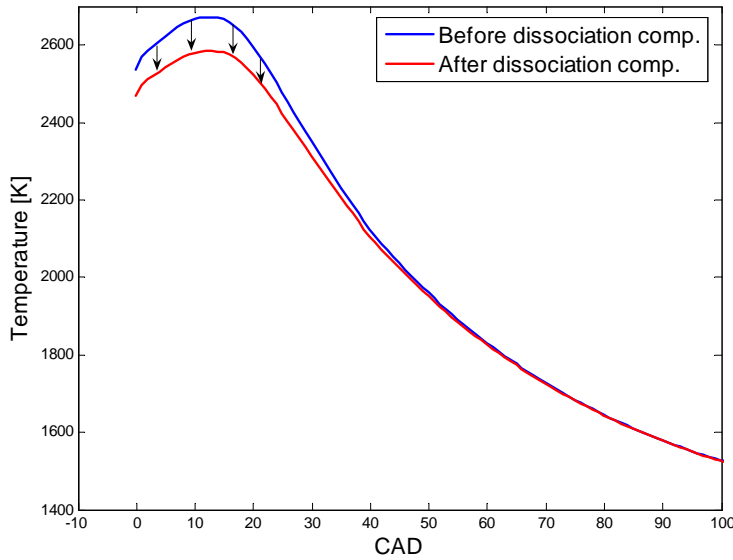


Figure 17 Typical burned zone temperature before and after dissociation compensation.

The NO formation is modelled using the Zeldovich mechanism equilibrium approach [6]. The (original) Zeldovich mechanism includes the following two reactions:



The equilibrium approach assumes that the residence time in the flame is short; therefore the NO formation takes place in the (post flame) burned zone only. This allows for a useful simplification; equilibrium concentrations are used for all species except for NO. Also assuming that the atomic nitrogen concentration is low and slowly varying, i.e.:

$$\frac{dc_N}{dt} = 0 \quad (3.22)$$

the following expression is derived:

$$\frac{dc_{NO}}{dt} = \frac{2r_1 \{1 - (c_{NO} / c_{NO,eq})^2\}}{1 + (c_{NO} / c_{NO,eq})r_1 / r_2} \quad (3.23)$$

where

$$r_1 = k_1^+ c_{O,eq} c_{N_2,eq} \quad (3.24)$$

$$r_2 = k_2^- c_{NO,eq} c_{O,eq} \quad (3.25)$$

denotes the forward/backward reaction rates of equations 3.20 and 3.21.

The equilibrium oxygen and nitrogen concentrations in the burned zone are given by look-up tables. This allows for fast calculations and eliminates the need to know the exact gas composition of the burned zone as in previous models [4].

3.3 Results

The engine-out NO_x model was validated using steady state measurement data collected in an engine test bed, a total of 29 points varying in load from idle to 100% load and in speed from 500 rpm to 2300 rpm.

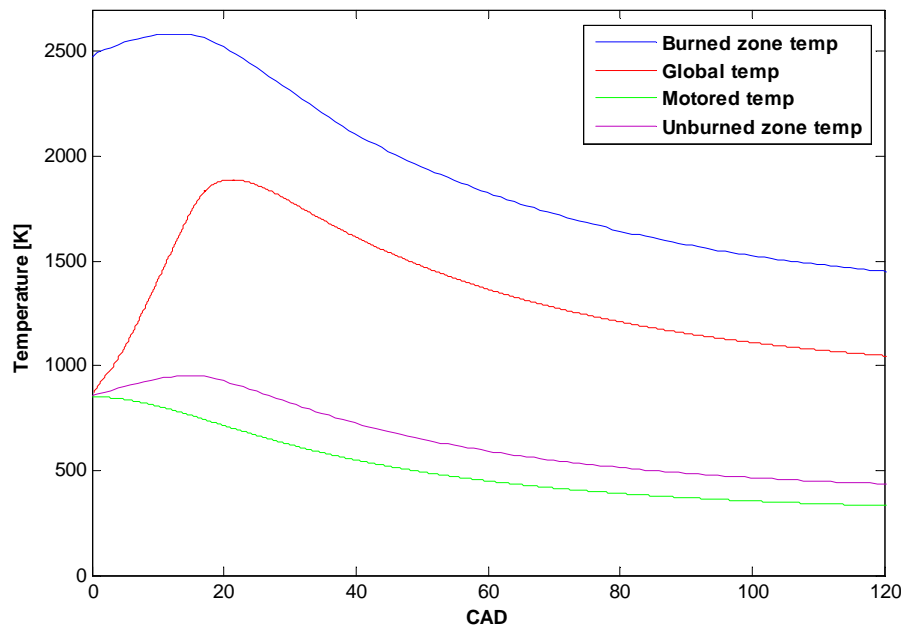


Figure 18 Typical combustion temperatures, 1000rpm / 100% load.

Figure 18 shows simulated combustion temperatures at 1000 rpm / 100 % load. The zone temperatures have not been validated on the specific test engine because of a lack of in-cylinder temperature measurements.

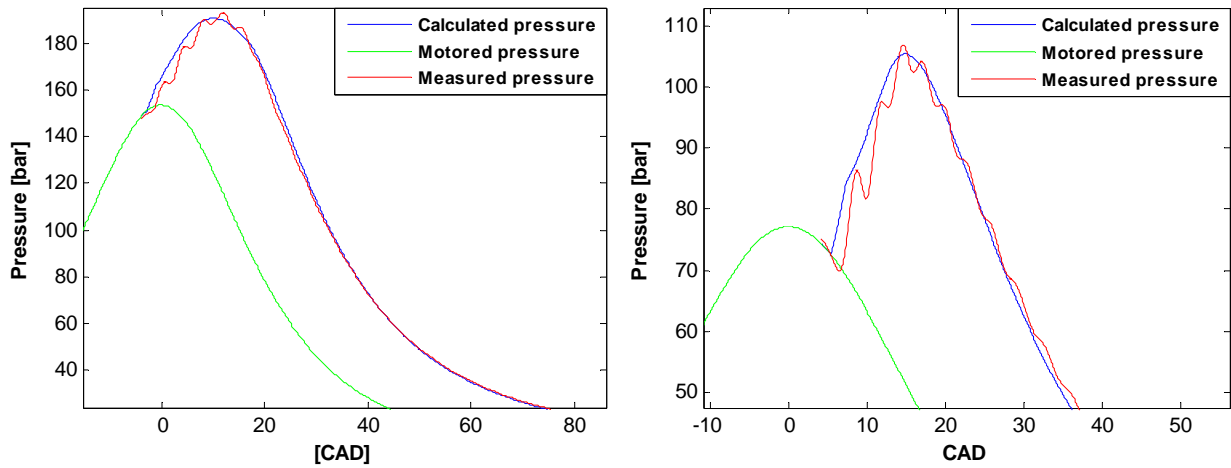


Figure 19 Measured and simulated cylinder pressure.

Two simulated pressure traces are compared with their measured counterparts in Figure 19. The agreement is satisfactory in both the first high load case and in the second medium load case. Peak pressure is predicted with good accuracy. The oscillations in the measurements, originating from pulsations in the channels where the pressure sensors are connected, make validation of ignition delay difficult however.

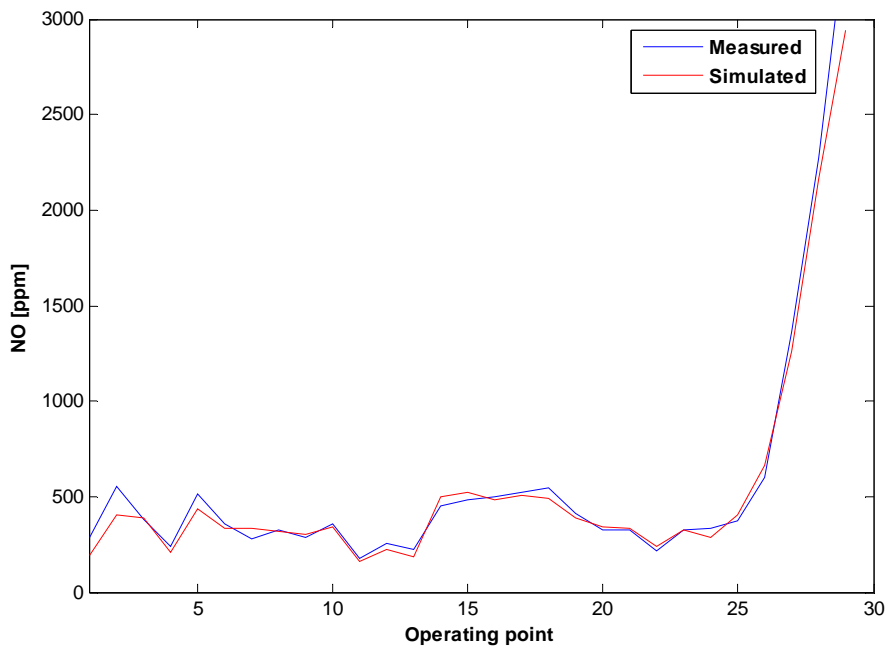


Figure 20 Simulated and measured NO_x.

Figure 20 shows measured and simulated NO_x for the steady state points studied. The agreement is quite good; the mean relative error is 10.4 %. The average simulation time is 50 ms per cycle on a 1.6 GHz computer which corresponds to real time performance up to 2400 rpm. This is substantially faster than previous models which required several minutes per cycle [4].

Indicated mean effective pressure (IMEP) is easily calculated from the simulated pressure trace. Using a simple second order polynomial depending on engine speed to

compensate for friction losses and auxiliary unit losses, torque can be estimated. The results are given in Figure 21 in the steady state case.

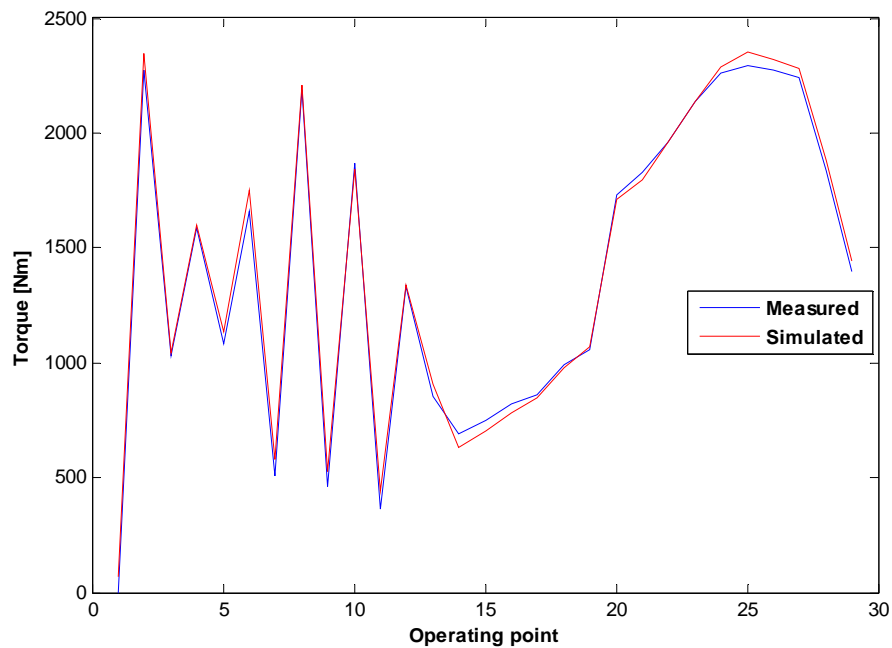


Figure 21 Simulated and measured torque.

Due to a lack of measurements, the exhaust temperature model was validated using another set of steady state data from an engine of the same type as in the previous set, although with a different calibration. A total of 120 points are included ranging in speed from 600 to 2300 rpm and in load from 0 to 100 %. The agreement between measured and calculated exhaust temperature is excellent, the results are given in Figure 22. The mean relative error is 1.7%. The highest deviation occurs at 0% load and low speeds (points 12-20); operating conditions where the NO_x flow is correspondingly extremely low.

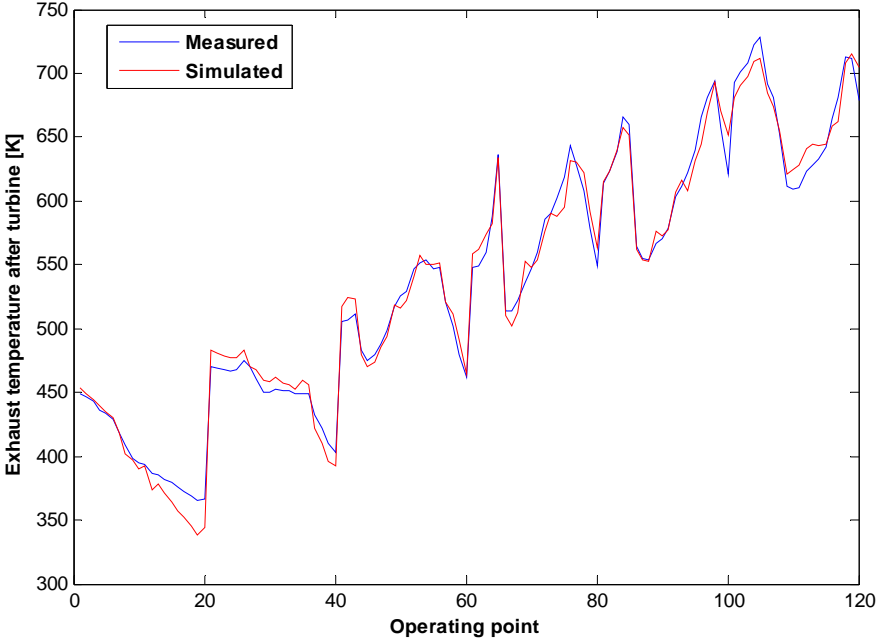


Figure 22 Simulated and measured exhaust temperature (after turbine).

4 Gas exchange model

A gas exchange model is a useful addition to the engine-out NO_x model. This allows for a complete engine modelling package.

4.1 The model

The gas exchange model uses a simple filling and emptying quasi steady concept. It was previously described by Ericson [11]. The model is schematically depicted in Figure 23.

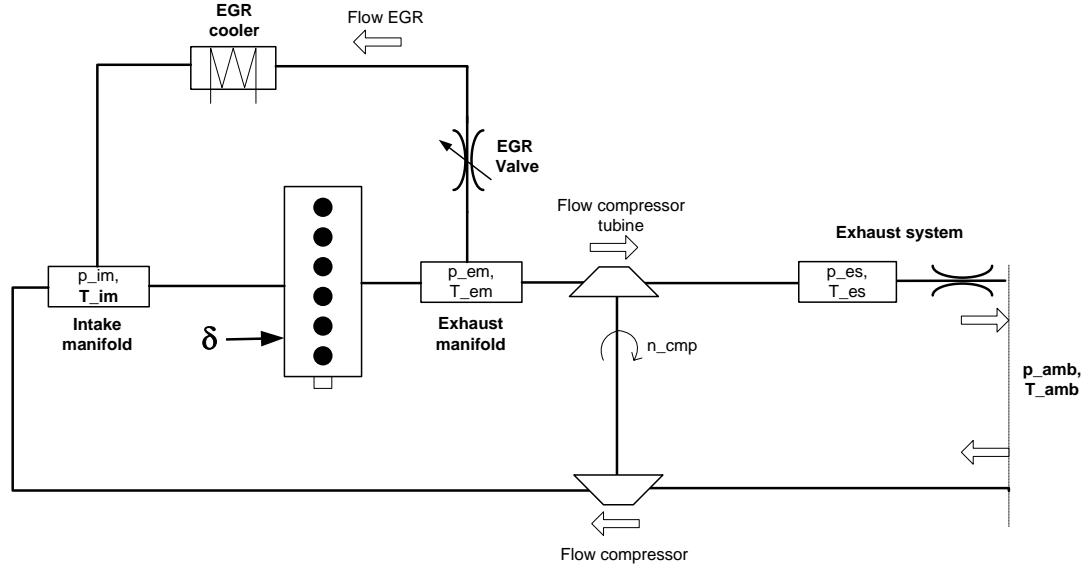


Figure 23 Schematic description of the gas exchange model.

All gas compositions are assumed to be constant, i.e. constant values for the specific heats are used. The intake manifold temperature is measured and is used as an input to the model. The reason is that it is difficult to model the charge air and EGR temperatures. Factors such as fouling of the coolers and wind conditions will affect these temperatures in onboard applications. In the laboratory using the modelled engine however, the intake manifold temperature varies in a very small range, typically 295-315 K. Simply setting the temperature to a constant value is a good simplification, as will be shown in the results section. The model is implemented in Simulink for optimum performance and uses a fixed time step length of 10 ms. Using longer steps, stability problems will occur.

The different sub models will be presented following the air/exhaust path through the engine, starting from the intake side.

4.1.1 Compressor

The mass flow and efficiency of the compressor is calculated using look-up tables:

$$W_{cmp} = W_{cmp} \left(\frac{p_{im}}{p_{amb}}, n_{cmp} \right) \quad (4.1)$$

$$\eta_{cmp} = \eta_{cmp} \left(\frac{p_{im}}{p_{amb}}, n_{cmp} \right) \quad (4.2)$$

The torque is given by:

$$M_{cmp} = \frac{W_{cmp} c_{p,air} T_{amb}}{\eta_{cmp} \omega_{cmp}} \cdot \left(\left(\frac{p_{im}}{p_{amb}} \right)^{\frac{\gamma_{air}-1}{\gamma_{air}}} - 1 \right) \quad (4.3)$$

T_{amb} and p_{amb} are the ambient temperature and pressure.

4.1.2 Intake and exhaust manifold

The intake manifold is described as a control volume (an open system of constant volume). By neglecting heat transfer, assuming a constant (slowly varying) temperature in the manifold and differentiating the ideal gas law and internal energies the following expression is achieved:

$$\dot{p}_{im} = \frac{R_{im}}{V_{im}} \cdot T_{im} (W_{cmp} + W_{egr} - W_{eng,in}) \quad (4.4)$$

The exhaust manifold is modelled analogously to the intake manifold:

$$\dot{p}_{em} = \frac{R_{exh}}{V_{em}} T_{em} (W_{eng,out} - W_{egr} - W_{trb}) \quad (4.5)$$

4.1.3 EGR system

The EGR flow is modelled using the expression for choked flow through a restriction, described by [6]:

$$W_{egr} = A_{egr} \cdot \frac{p_{em}}{\sqrt{T_{em} R_{exh}}} \cdot \psi \left(\frac{p_{im}}{p_{em}}, \gamma_{exh} \right) \quad (4.6)$$

where

$$\psi \left(\frac{p_{im}}{p_{em}}, \gamma_{exh} \right) = \begin{cases} \sqrt{\frac{2\gamma_{exh}}{\gamma_{exh}-1} \left(\left(\frac{p_{im}}{p_{em}} \right)^{\frac{2}{\gamma_{exh}}} - \left(\frac{p_{im}}{p_{em}} \right)^{\frac{\gamma_{exh}+1}{\gamma_{exh}}} \right)} & \text{if } \frac{p_{im}}{p_{em}} \geq \xi \\ \sqrt{\gamma_{exh} \left(\frac{2}{\gamma_e + 1} \right)^{\frac{\gamma_{exh}+1}{\gamma_{exh}-1}}} & \text{if } \frac{p_{im}}{p_{em}} < \xi \end{cases} \quad (4.7)$$

$$\xi = \left(\frac{2}{\gamma_e + 1} \right)^{\frac{\gamma_{exh}}{\gamma_{exh}-1}}$$

A_{egr} is the effective flow area of the EGR valve, a function of the valve control signal u_{egr} (using a look-up table):

$$A_{egr} = A_{egr}(u_{egr}) \quad (4.8)$$

4.1.4 Turbine

The mass flow and efficiency of the turbine are also calculated using look-up tables:

$$W_{trb} = f_{W_{trb}} \left(\frac{p_{em}}{p_{es}}, n_{trb}, u_{vgt} \right) \quad (4.9)$$

$$\eta_{trb} = f_{\eta_{trb}} \left(\frac{p_{em}}{p_{es}}, n_{trb}, u_{vgt} \right) \quad (4.10)$$

u_{vgt} is the control signal of the variable geometry turbocharger (VGT). The torque and temperature after the turbine are given by:

$$M_{trb} = \frac{\eta_{trb} W_{trb} c_{p,exh} T_{em}}{\omega_{trb}} \cdot \left(1 - \left(\frac{p_{em}}{p_{es}} \right)^{\frac{1-\gamma_{exh}}{\gamma_{exh}}} \right) \quad (4.11)$$

$$T_{trb} = \left(1 + \eta_{trb} \left(\left(\frac{p_{em}}{p_{es}} \right)^{\frac{1-\gamma_{exh}}{\gamma_{exh}}} - 1 \right) \right) \cdot T_{em} \quad (4.12)$$

The turbine speed is calculated using:

$$\dot{n}_{trb} = \frac{60}{2\pi J_{trb}} \cdot (M_{trb} - M_{cmp}) \quad (4.13)$$

where J_{trb} is the inertia of the turbocharger.

4.1.5 Exhaust system

The exhaust system is modelled using a control volume (analogously to the intake and exhaust manifold):

$$\dot{p}_{es} = \frac{R_{exh}}{V_{es}} T_{es} (W_{trb} - W_{es}) \quad (4.14)$$

A quadratic restriction describes the exhaust mass flow:

$$W_{es}^2 = \frac{p_{es}}{k_{es} R_{exh} T_{trb}} (p_{es} - p_{amb}) \quad (4.15)$$

where k_{es} is the restriction constant and $T_{es} = T_{trb}$.

4.1.6 Exhaust temperature

The exhaust (manifold) temperature is modelled using a static model:

$$T_{em} = T_{im} + \frac{Q_{LHV} f_{exh} (W_{fuel}, n_{eng})}{c_{p,exh} (W_{eng,in} + W_{fuel})} \quad (4.16)$$

where T_{im} is the inlet manifold temperature, W_{fuel} the fuel mass flow, $W_{eng,in}$ the total mass flow (EGR + charge air) into the engine. f_{exh} is a look-up table. Note that this model only gives accurate results for a given engine calibration; effects of varying injection timing and delta can not be studied.

4.2 Results

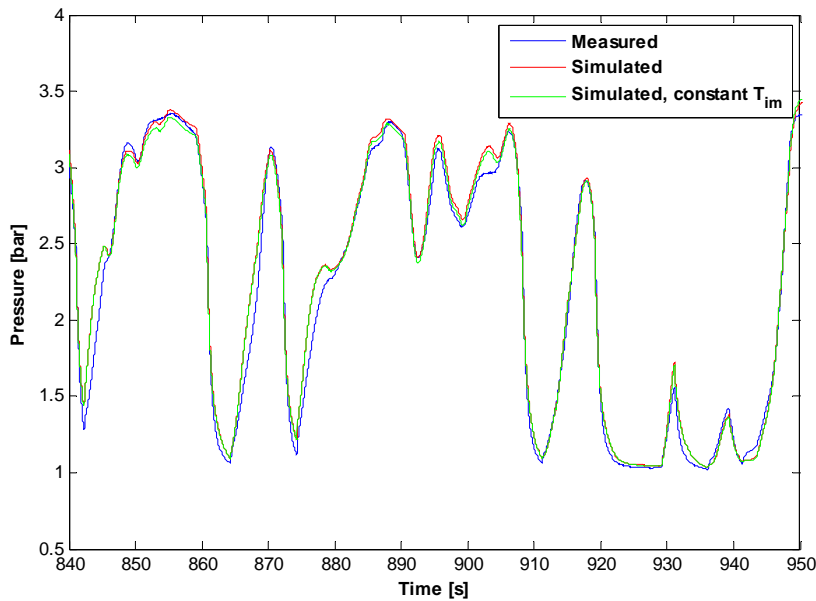


Figure 24 Simulated and measured inlet manifold pressure, sequence of the ETC.

Despite the simplicity of the gas exchange model, it provides good agreement with measurements. The agreement between simulated and measured inlet manifold pressure is adequate, Figure 24 shows a sequence of the ETC. The mean relative error over the ETC is 5.9 %.

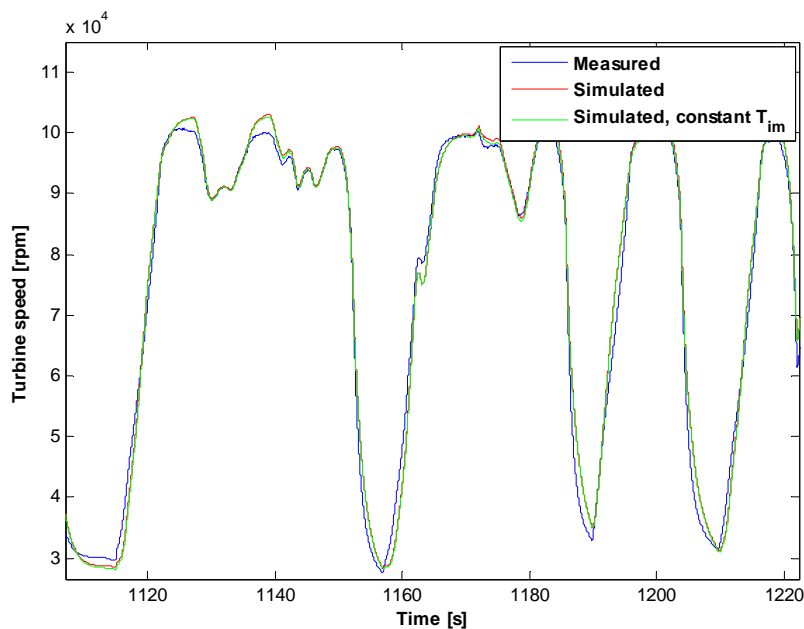


Figure 25 Simulated and measured turbine speed, sequence of the ETC.

Equally good results are achieved for the simulated turbine speed; another sequence of the ETC is shown in Figure 25. Figure 24 and Figure 25 also illustrates that the model is not very sensitive for small changes in inlet manifold temperature. A constant value of 304 K (green curve) shows little deviation from when the measured temperature is used (red curve). The simulation time is faster than 100 times real time.

5 Complete engine model

The engine-out NO_x model is combined with the gas exchange model to form a complete engine model. The combined model does not require measured pressures, temperatures or EGR rates to predict the emissions.

5.1 Model structure

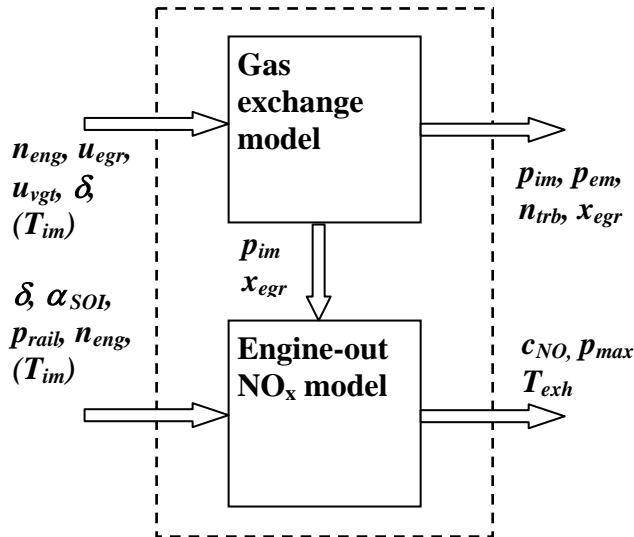


Figure 26 Inputs and outputs of the complete model.

The model structure is illustrated in Figure 26. The inputs are engine speed, injected fuel amount, injection timing, rail pressure, EGR valve position and VGT actuator position i.e. the typical engine control parameters available in the engine control system. A large number of output signals are possible. Typical outputs are inlet and exhaust manifold pressure, EGR rate, NO concentration, peak cylinder pressure and exhaust temperature. Note that the models are not fully integrated in the sense that two exhaust temperature models are used in parallel. The Gas Exchange Model must use a short 10 ms step in order to remain stable. At the same time, it is desirable to run the engine-out NO_x model much more sparsely in order to save computational time. For a given engine calibration, to which the static exhaust temperature model of the Gas Exchange Model is properly tuned, excellent results can be achieved as will now be discussed.

5.2 Results

NO_x measurements during the European Transient test Cycle (ETC) were performed on the test engine. Two sequences of the test cycle are shown in Figure 27 and Figure 28.

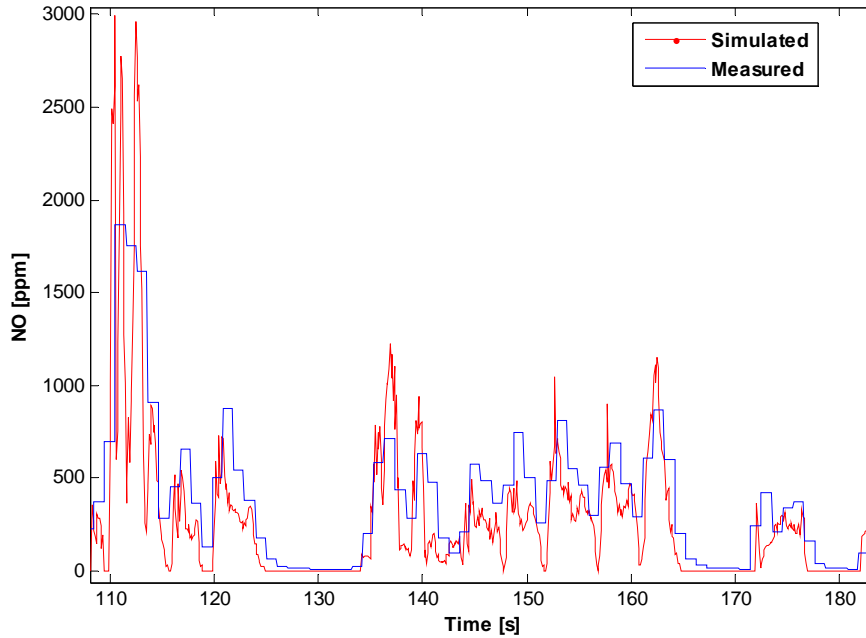


Figure 27 Measured and simulated NO_x, sequence of the ETC.

The measurements are smoothed because of mixing in the pipes leading to the gas analyzer and the sampling rate is only 1 Hz. Still, we can conclude that the agreement between measured and simulated emissions is adequate for the intended application. Specific NO_x emissions for the complete cycle show a relative error of 7.14 % to measured data. Note that the calibration of the engine-out NO_x model was performed with a relatively small data amount (the 29 steady state points previously discussed). Even better results can likely be achieved with a set of steady state data more representative of the ETC.

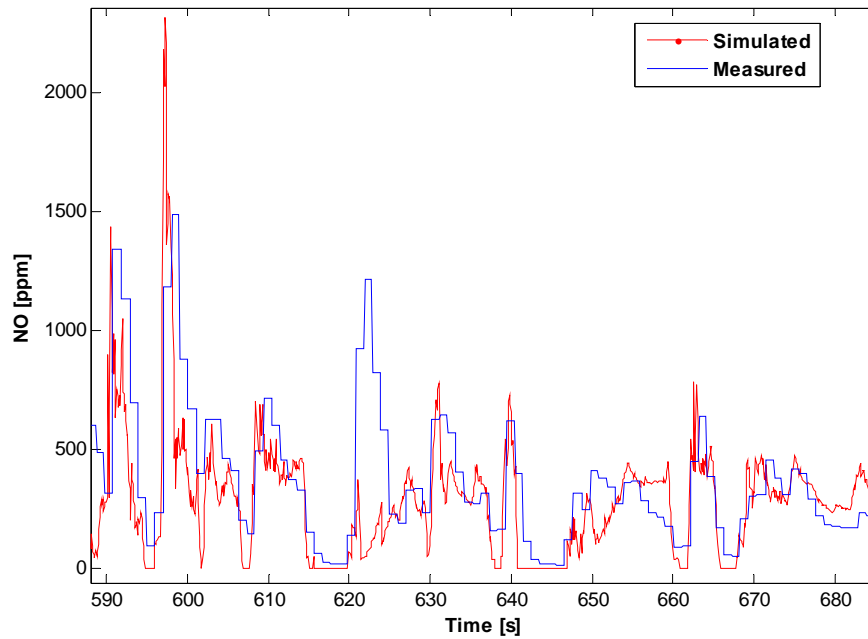


Figure 28 Measured and simulated NO_x, sequence of the ETC.

The simulation time for a complete ETC using a 10Hz update interval is less than 15 minutes; in other words 2 times real time performance. This makes the engine model a suitable candidate for control and optimization purposes. The transient performance of the exhaust temperature model is validated in chapter 7.

6 SCR catalyst model

In this chapter, a model of a vanadium based unsupported SCR catalyst of typical heavy truck dimensions is presented. The catalyst is modelled as a series of continually stirred tank reactors. The walls are discretized into a number of layers to describe the mass transport through the walls, as illustrated in Figure 29. The model uses 2 wall layers and 6 segments (tanks) in the axial direction. One temperature state in each tank and one ammonia coverage in each wall layer results in a total of 18 states. This is a less dense discretization than traditionally used, Westerberg et al. for example uses 10 tanks in the axial direction [12].

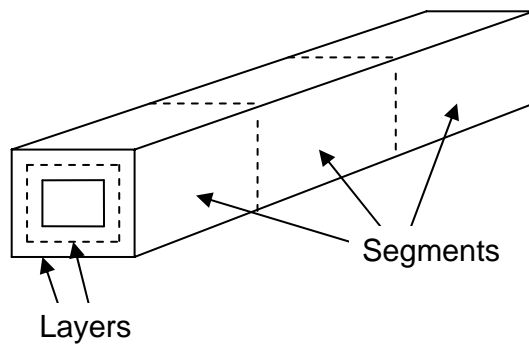
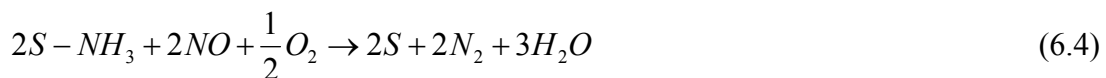


Figure 29 Illustration of the catalyst discretization principle.

Uniform radial flow and concentration distribution over the catalyst cross section is assumed; therefore it is sufficient to model one channel only. Axial diffusion and the radial temperature gradients are both neglected.

6.1 Reactions

The reaction mechanism consists of five reactions:



S denotes an active site on the catalyst surface. Reaction 1 (equation 6.1) describes the decomposition of Urea to ammonia. This is a simplification; the actual decomposition consists of two reactions. First the urea is decomposed in gas phase to equimolar amounts of ammonia and isocyanic acid (thermolysis). Then the isocyanic acid is hydrolyzed to ammonia on the catalyst surface. This step is generally considered to be fast compared to the thermolysis; therefore it is a reasonable assumption to treat the isocyanic acid as ammonia. The adsorption / desorption (accumulation) of ammonia is given by reactions 2 and 3 (equations 6.2 and 6.3). Traditionally, the activation energy for desorption of ammonia is considered to be reduced with increasing coverage. This

can be modelled as a Temkin-type isotherm with linearly decreasing activation energy [13]. Another approach is to use two different types of sites with different activation energy. In the kinetic model given here however, only one site type is used with constant activation energies. The desired reaction, NO-reduction on the active sites is described by reaction 4 (equation 6.4). Finally, at higher temperatures, unwanted ammonia oxidation also occurs on the sites, reaction 5 (equation 6.5). The corresponding reaction rates are given by:

$$r_1 = k_1 c_{Urea} \quad (6.6)$$

$$r_2 = k_2 c_{NH_3} (1 - \theta_{NH_3}) \quad (6.7)$$

$$r_3 = k_3 \theta_{NH_3} \quad (6.8)$$

$$r_4 = k_4 c_{NO} \theta_{NH_3} \quad (6.9)$$

$$r_5 = k_5 \theta_{NH_3} \quad (6.10)$$

The rate coefficients k_j are calculated using an Arrhenius type expression:

$$k_j = k_{0,j} e^{\frac{E_{A,j}}{RT_S}} \quad (6.11)$$

where j is reaction number, $k_{0,j}$ is the pre exponential factor, $E_{A,j}$ is the activation energy, R is the molar gas constant and T_S is the surface temperature.

6.2 Mass and heat balances

The axial flow and the radial diffusion are both modelled using static balance equations for the gas phase and time dependent balances for the solid catalyst.

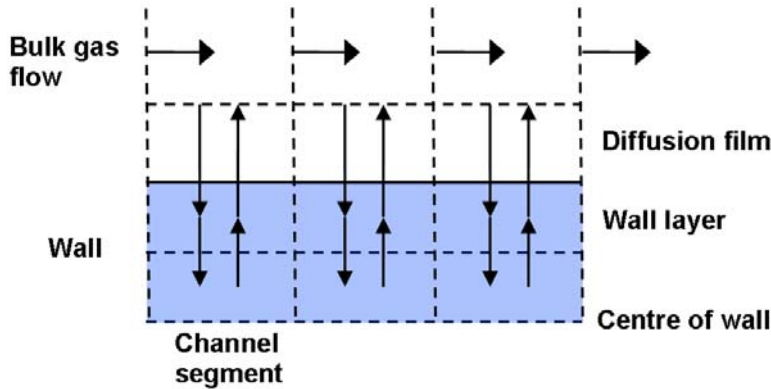


Figure 30 Illustration of mass transport in the catalyst channel.

The gas phase mass transport is illustrated in Figure 30 and is given mathematically by the following relations:

$$F_{tot} (y_{i,k-1} - y_{i,k}) - \Gamma_{i,k,0} (c_{i,k,0} - c_{i,k,1}) = 0 \quad (6.12)$$

$$\Gamma_{i,k,n-1} (c_{i,k,n-1} - c_{i,k,n}) - \Gamma_{i,k,n} (c_{i,k,n} - c_{i,k,n+1}) + \sum_j v_{i,j} r_{j,k,n} w_{k,n} = 0 \quad \text{for } n \geq 1 \quad (6.13)$$

where F_{tot} is the total molar flow $c_{i,k,n}$ is the concentration of component i in channel segment k and wall layer n (where $n=0$ indicates gas bulk and $n>0$ indicates wall) and $w_{k,n}$ is the mass of catalyst material in channel segment k and wall layer n . The mass transfer coefficients $\Gamma_{i,k,n}$ are given by:

$$\Gamma_{i,k,0} = \frac{A_k}{\frac{1}{k_{c,i,k}} + \frac{0.5\Delta x_1}{D_{eff,i,k}}} \quad (6.14)$$

$$\Gamma_{i,k,n} = \frac{D_{eff,i,k} A_k}{0.5\Delta x_n + 0.5\Delta x_{n+1}} \quad \text{for } n=1 \dots N-1 \quad (6.15)$$

$$\Gamma_{i,k,N} = 0 \quad (6.16)$$

where A_k is the mass and heat transfer area in channel segment k . For simplicity reasons, A_k is assumed to be constant for all wall layers. $D_{eff,i,k}$ is the effective pore diffusion coefficient of component i in channel segment k , $k_{c,i,k}$ is the film transfer coefficient of component i in channel segment k and Δx_n is the thickness of wall layer n . The gas energy balance is given by:

$$F_{tot} c_{p,g} (T_{g,k-1} - T_{g,k}) - h_k A_k (T_{g,k} - T_{s,k}) = 0 \quad (6.17)$$

where $c_{p,g}$ is the specific heat capacity for the gas, h_k is the heat transfer coefficient in channel segment k , $T_{g,k}$ and $T_{s,k}$ are the temperatures in channel segment k in the gas bulk and of the catalyst respectively. The solid energy balance is given by:

$$m_{s,k} c_{p,s} \frac{dT_{s,k}}{dt} = h_k A_k (T_{g,k} - T_{s,k}) - A_s (q_{k+1} - q_k) + \sum_n \sum_j r_{j,k,n} w_{k,n} (-\Delta H_j) \quad (6.18)$$

where $m_{s,k}$ is the total mass of solid material in channel segment k , $c_{p,s}$ is the heat capacity of the solid material, A_s is the cross sectional area of the catalyst wall, $w_{k,n}$ is the mass of active catalyst material in channel segment k and wall layer n and $-\Delta H_j$ is the heat of reaction j . The solid heat flux is calculated as:

$$q_k = -2\lambda_s \frac{T_{s,k} - T_{s,k-1}}{\Delta z_k + \Delta z_{k-1}} \quad \text{for } k = 2 \dots K-1, K \quad (6.19)$$

$$q_k = 0 \quad \text{for } k = 1, K+1 \quad (6.20)$$

where λ_s is the heat conductivity for the solid material, Δz_k is the length of channel segment k and K is the total number of channel segments. The mass and heat transfer is described with the film model and the mass and heat transfer coefficients are given by:

$$k_{c,i,k} = \frac{Sh D_{i,k}}{d} \quad (6.21)$$

$$h_k = \frac{Nu \lambda_g}{d} \quad (6.22)$$

where $D_{i,k}$ is the diffusion coefficient for component i in channel segment k , $\lambda_{g,k}$ is the gas heat conductivity in channel segment k and d is the channel width. Sh and Nu are the Sherwood and the Nusselt number respectively. The asymptotic values for Sh and Nu are used (entrance effects are neglected).

The surface mass balance for segment k and layer n is traditionally given by:

$$\frac{d\theta_{NH_3,k,n}}{dt} = \frac{1}{N_c} (r_{2,k,n}(t) - r_{3,k,n}(t) - 2r_{4,k,n}(t) - 2r_{5,k,n}(t)) \quad (6.23)$$

Using implicit methods, more accurate steps are given which allows for longer step lengths. The implicit calculations applied in the SCR model use the second layer concentrations and surface temperatures from the previous time step. Combining the updated first layer coverage according to:

$$\theta_{NH_3,k,1}(t + \Delta t) = \theta_{NH_3,k,1}(t) + \Delta t \frac{d\theta_{NH_3,k,1}}{dt} \quad (6.24)$$

with equations 6.14-6.16 and 6.23, the result is a third degree polynomial:

$$\beta_1 \left(\frac{d\theta_{NH_3,k,1}}{dt} \right)^3 + \beta_2 \left(\frac{d\theta_{NH_3,k,1}}{dt} \right)^2 + \beta_3 \left(\frac{d\theta_{NH_3,k,1}}{dt} \right) + \beta_4 = 0 \quad (6.25)$$

where

$$\beta_m = \beta_m(\Delta t, \theta_{NH_3,k,1}(t), c_{i,k-1,0}(t + \Delta t), c_{i,k-1,2}(t), F(t + \Delta t), T_s(t)) \quad (6.26)$$

The polynomial is easily solved using analytical methods. Choosing which root to use is simple; only one is physically possible.

Another method to improve high temperature stability is to simplify the system to a first order system approaching a steady state solution θ_{ss} in each time step [14]. The coverage is given by:

$$\frac{d\theta_{NH_3,k,1}}{dt} = \frac{\theta_{ss,k,1} - \theta_{NH_3,k,1}}{\tau} \quad (6.27)$$

where $\theta_{ss,k,1}$ is the steady state solution corresponding to the current inputs and τ is a characteristic time constant.

The steady state solution can be estimated by solving a simplified version of the gas phase mass balances (equations 6.12-6.13). At high temperatures the system is mass transport limited which allows for a number of simplifications. The simplifications consist of assuming that all urea is decomposed and all ammonia reacts with NO before reaching the second layer. Also, a simple approximation for the second layer NO concentration is applied:

$$c_{NO,k,2} = \max(0, c_{NO,k-1,0} - c_{NH_3,k-1,0} - 2c_{Urea,k-1,0}) \quad (6.28)$$

By combining the simplified gas phase mass balances with equilibrium in the surface mass balances, i.e:

$$r_{2,k,1} - r_{3,k,1} - 2r_{4,k,1} - 2r_{5,k,1} = 0 \quad (6.29)$$

, the result is a third degree polynomial:

$$\alpha_1 (\theta_{ss,k,1})^3 + \alpha_2 (\theta_{ss,k,1})^2 + \alpha_3 (\theta_{ss,k,1}) + \alpha_4 = 0 \quad (6.30)$$

where:

$$\alpha_m = \alpha_m(c_{i,k-1,0}(t + \Delta t), F(t + \Delta t), T_s(t)) \quad (6.31)$$

This polynomial is also solved using analytical methods, and only one root is physically possible. Note that the simplifications are only valid at high temperatures. Empirically, for the catalyst studied, it has been shown that above approximately 700 K, the simplifications result in good accuracy. The time constant is estimated using a black box model:

$$\tau_{k,1} = \tau_{k,1}(T_{s,k}, \theta_{ss,k,1}, c_{NO,k,1}, c_{NH_3,k,1}, c_{Urea,k,1}) \quad (6.32)$$

The two methods are combined in the model with a switching point of 720K.

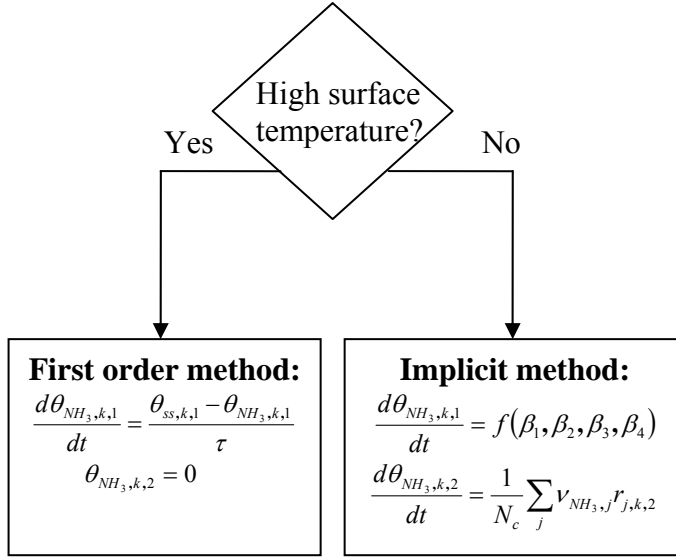


Figure 31 Illustrating the two different coverage updating methods.

The gas diffusivity for each component i is calculated using a simplified form of the Fuller-Schettlet-Giddins equation [14]:

$$D_i = D_{ref,i} \left[\frac{T_s}{T_{ref}} \right]^{1.75} \quad (6.33)$$

where T_{ref} is a reference temperature. The effective diffusivity for pore diffusion is given as:

$$D_{eff,i} = \frac{f_D}{\frac{1}{D_i} + \frac{1}{D_{K,i}}} \quad (6.34)$$

f_D is a factor that takes into consideration the porosity and the tortuosity of the porous material. $D_{K,i}$ is the Knudsen diffusivity which is calculated as:

$$D_{K,i} = \frac{d_p}{3} \sqrt{\frac{8RT_s}{\pi M_i}} \quad (6.35)$$

where d_p is the mean pore diameter.

6.3 Urea decomposition before the catalyst

Heating the urea to exhaust temperature and vaporizing it will result in a temperature drop according to:

$$T_{cat,in} = T_{precat} - \frac{y_{urea}}{c_{p,exh}} \left(H_{v,urea} + x_{H_2O} H_{v,H_2O} + (c_{p,urea} + x_{H_2O} c_{p,H_2O}) (T_{precat} - T_{amb}) \right) \quad (6.36)$$

x_{H_2O} is the molar ratio of water to urea and $H_{v,urea} / H_{v,H_2O}$ is the heat of vaporization of urea / water.

Thermolysis will also occur in the gas phase after the urea injection and before the catalyst. A first order reaction mechanism is applied:

$$r_{precat} = k_{precat} c_{urea} \quad (6.37)$$

The rate coefficient is given by:

$$k_{precat} = k_{0,precat} e^{-\frac{E_{A,precat}}{RT_{cat,in}}} \quad (6.38)$$

The conversion is calculated using a tubular reactor model:

$$x = 1 - e^{-\frac{k_{precat} V_{precat}}{W_{exh}}} \quad (6.39)$$

where V_{precat} is the exhaust system volume between the injector and the catalyst inlet and W_{exh} is the total exhaust gas mass flow.

6.4 Results

The SCR catalyst model is validated using a number of step response experiments and a measured ETC.

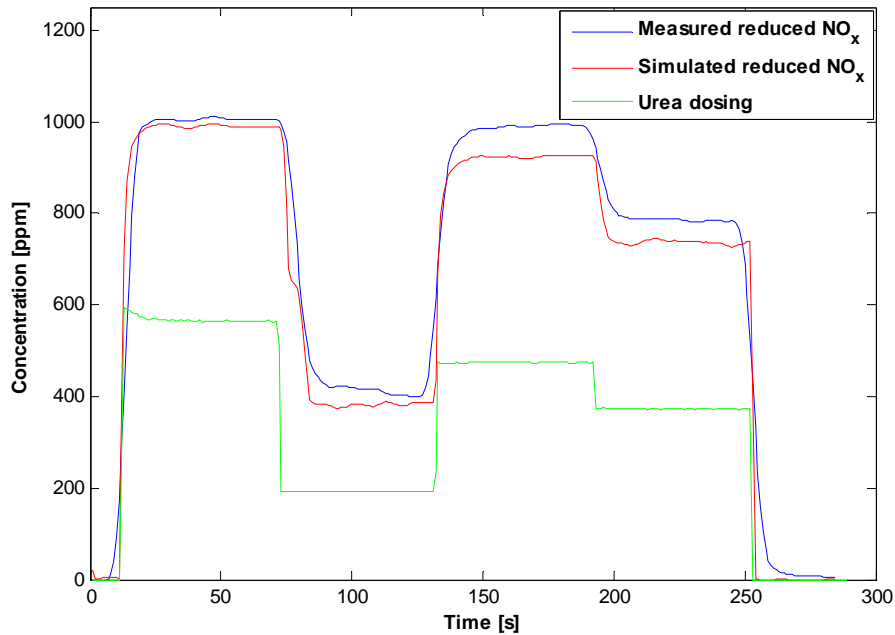


Figure 32 Simulated and measured NO_x reduction, step response experiment at 670 K.

The first step experiment is performed at constant exhaust temperature (670 K), flow (8 mole/s) and NO_x concentration (1000 ppm) with steps in the urea dosing. The results are given in Figure 32. The agreement is good considering the simplicity of the model. The plateau in simulated NO_x around 80 s is related to mass transport between the two wall layers. Using three or more wall layers, this effect would not be apparent.

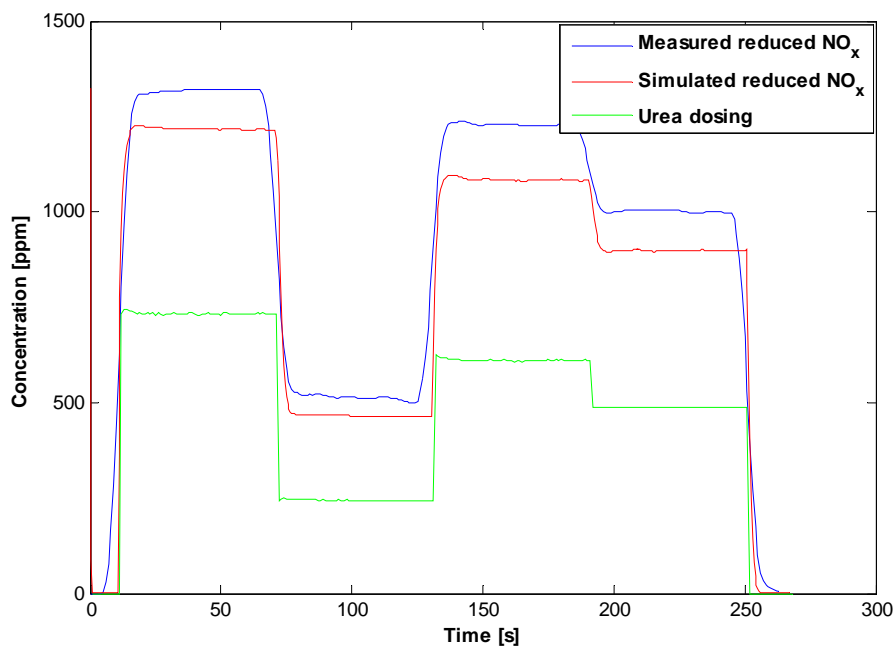


Figure 33 Simulated and measured NO_x reduction, step response experiment at 760 K.

The second step experiment is similar to the first except for a higher exhaust temperature of 760 K. The model will operate using the first order method under these conditions. The deviation between measured and simulated emissions is larger than in the first experiment but still reasonable considering the operating conditions.

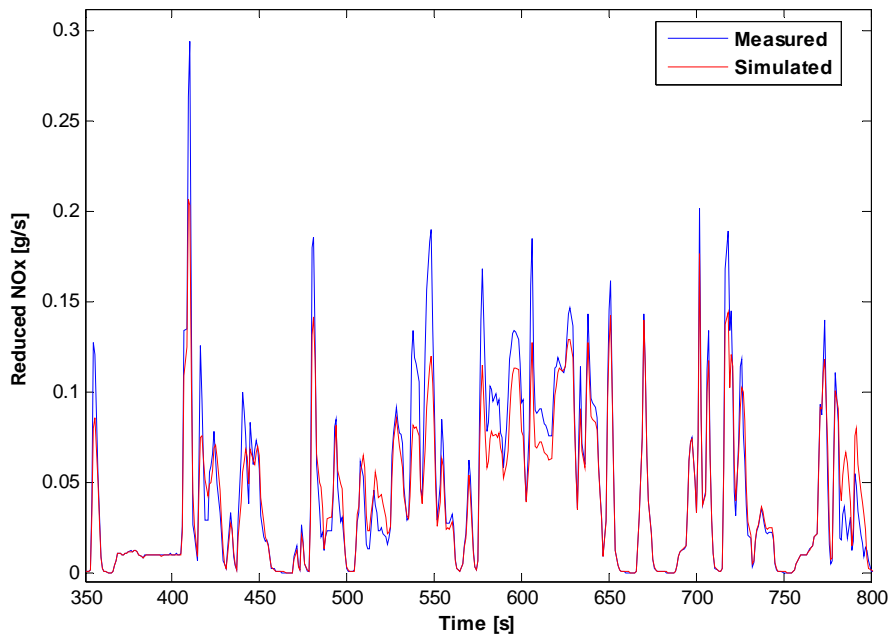


Figure 34 Simulated and measured NO_x reduction, sequence of the ETC.

The ETC measurements were performed with an engine calibrated for low engine-out NO_x levels and a low exhaust temperature of less than 650 K in all points. Simulated and measured NO_x during a sequence of the ETC is given in Figure 34. The agreement is excellent, and is on par with previous more complex models [15, 16]. Specific NO_x emissions after the catalyst are predicted with a 5.7 % relative error.

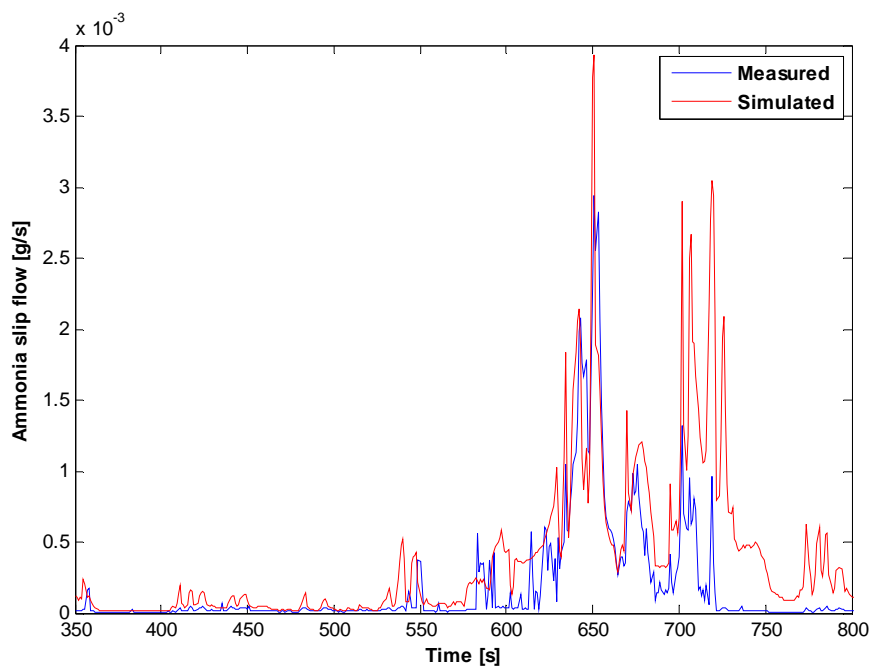


Figure 35 Simulated and measured ammonia slip, sequence of the ETC.

The ammonia slip, i.e. the ammonia flow after the catalyst, is predicted with reasonable accuracy. The results are given in Figure 35 for a sequence of the ETC. The mean ammonia slip concentration is underestimated by 40.5 %.

The combined use of implicit and first order methods allows for a 0.5s time step. The simulation time for a complete ETC is 20.8 s on a 1.6 GHz PC using uncompiled Matlab code. This corresponds to almost 100 times real time which makes the SCR catalyst model suitable for the intended purpose.

7 Combined engine and SCR catalyst model

The previously described engine and SCR catalyst models are combined to form a complete model of the system.

7.1 Model structure

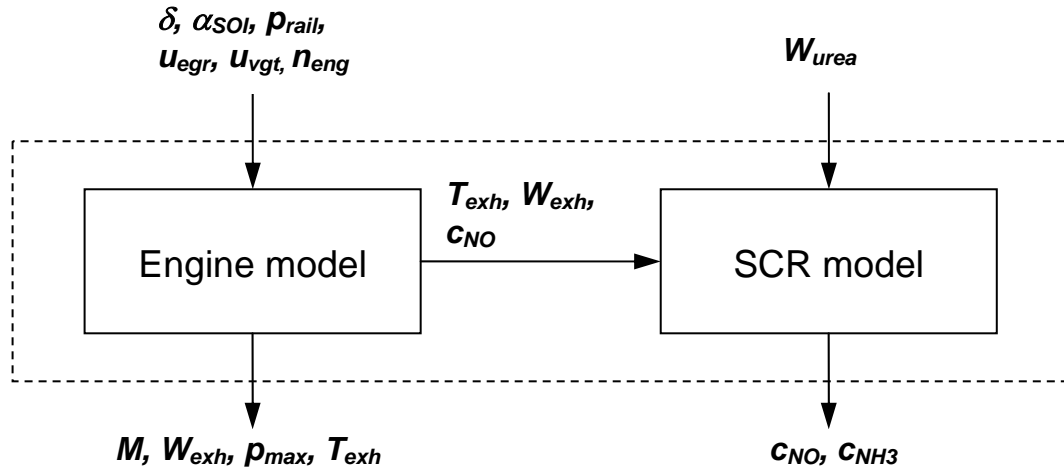


Figure 36 Model structure.

The model structure of the combined engine and SCR model is given in Figure 36. The only inputs required are the typical engine control parameters. Torque, exhaust flow and NO concentration are given as outputs. Peak cylinder pressure is also given which is useful during optimization to ensure that the physical limitations of the engine are not exceeded.

7.2 Results

Validation was performed by running an ETC on a six cylinder experimental engine equipped with cooled EGR, common rail fuel injection and a urea SCR system. The gas exchange model was not properly tuned to the test engine at the time of writing, therefore measured inlet manifold pressure and EGR rate is used. The exhaust temperature model was slightly re-tuned to improve the fit to the experimental engine. Also note that the test engine uses pilot injections in many operating cases. The engine-out NO_x model does not include this feature at the moment; therefore it was ignored and considered a part of the main injection.

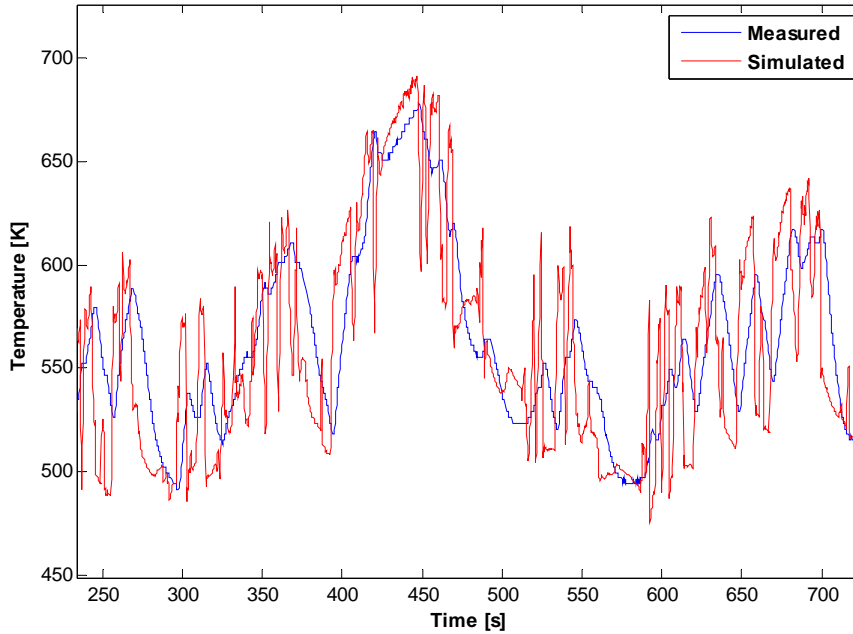


Figure 37 Simulated and measured exhaust temperature before catalyst.

The exhaust temperature model gives a reasonable fit to measured values; a sequence of the ETC is given in Figure 37. The slow dynamics of the temperature sensor is likely one of the explanations of the deviation. Heat transfer between the exhaust system and the temperature sensor will also contribute to the smoothed appearance of measured temperature.

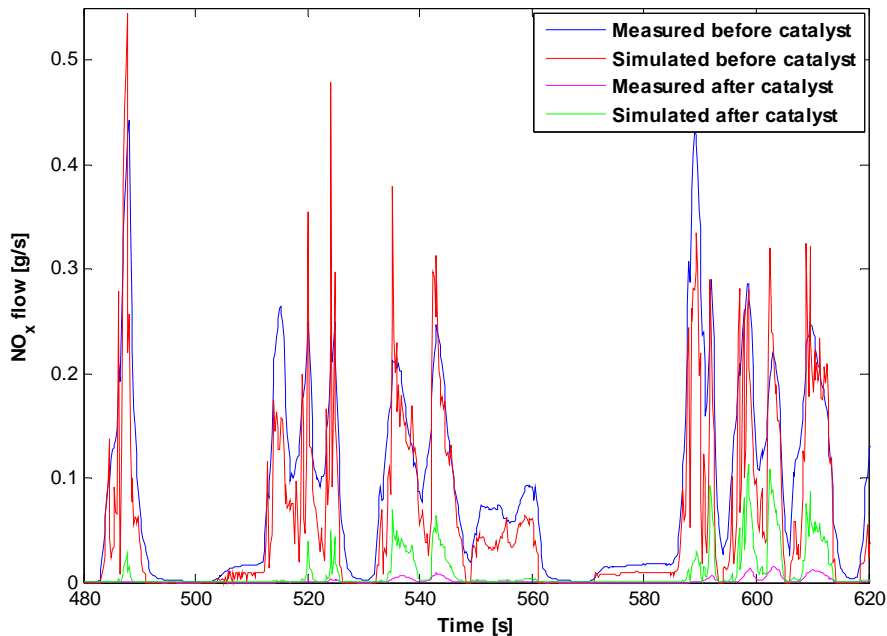


Figure 38 Simulated and measured NO_x before and after catalyst, sequence of the ETC.

Engine-out NO_x is predicted with excellent accuracy (Figure 38); the agreement is almost on par with the results presented in Chapter 5, specific NO_x over the cycle is under-estimated with 15.4 %. The pilot injections used on the test engine is likely one of the explanations of the higher deviation from measured data compared to previous

simulations. Tailpipe NO_x (after the catalyst) is over-estimated however; in other words, the SCR catalyst model under-estimates the conversion.

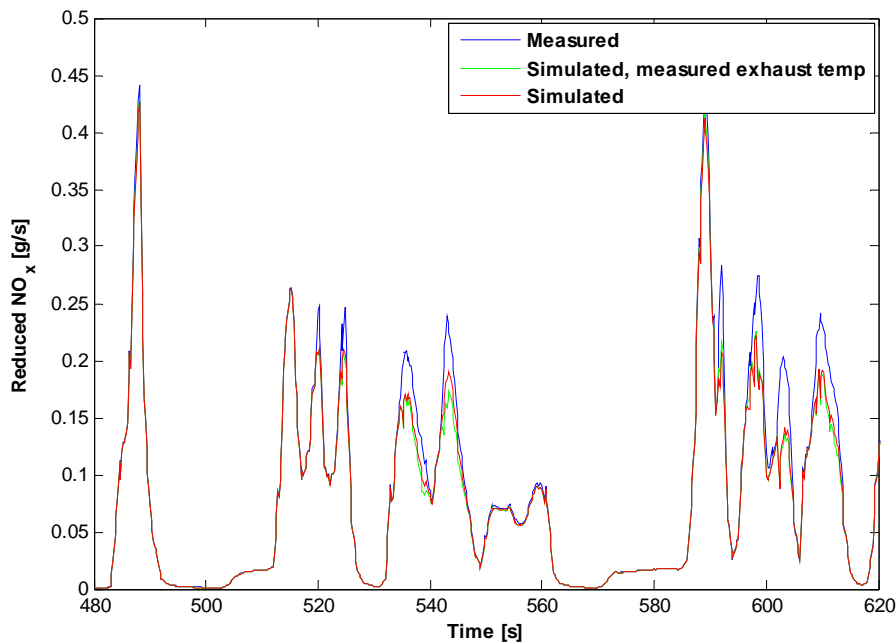


Figure 39 Simulated and measured reduced NO_x over the catalyst, sequence of the ETC.

Note that the conversion is extremely high in the experiment though which makes the absolute NO_x values after the catalyst very low. This means that the relative error is quite large even though the simulated conversion over the catalyst, as depicted in Figure 39, looks adequate. Reduced specific NO_x (relative to measured engine-out NO_x) is under-estimated with 8.7 %. One factor which could explain the under-estimated reduction is that the pre catalyst urea decomposition model lacks in transient accuracy. This makes the tuning process of the catalyst model less successful. Figure 39 also shows a comparison between the NO_x reduction as given by the SCR catalyst model with measured and simulated exhaust temperature; the difference is negligible. This is expected since the catalyst in it self has rather slow dynamics; the rapid fluctuations in simulated exhaust temperature does not result in equally rapid changes in catalyst temperature.

8 Summary

Extremely computationally efficient models for diesel engine combustion / NO_x formation, gas exchange in a diesel engine and NO_x reduction using an SCR catalyst are presented.

The first step involved developing quasi steady emission prediction methods. A physically based correction method termed the Delay Model is presented. The Delay Model is based on estimating a turbo charger delay time during transients to calculate a dynamic air-fuel equivalence ratio. Using this compensated value, transient correction factors can be calculated to predict carbon monoxide and particulate emissions with reasonable accuracy on Euro III class diesel engines. The models lack in accuracy to be used for simulation / optimization purposes however.

Improved accuracy of engine-out NO_x predictions was achieved by developing a zero dimensional combustion and NO_x formation model. The cylinder contents are divided into one unburned zone consisting of air and EGR and one burned zone containing the results of perfect combustion. The model is predictive, i.e. the heat release rate is predicted using fuel injection parameters. The burned zone temperature is calculated in two steps, first assuming perfect combustion, and secondly compensating this value for incomplete combustion using tabulated data. NO_x formation is calculated according to the original Zeldovich mechanism. Tabulated data describing the equilibrium concentrations in the burned zone are used to speed up calculations. The average calculation time is 50 ms per cycle.

In addition to the engine-out NO_x model, a gas exchange model of the quasi-steady filling and emptying type is presented. A total of 4 states are used to describe the gas flows and temperatures in the diesel engine. The modelled engine includes an EGR system and a variable geometry turbocharger (VGT). The model requires a 10ms time step length to remain stable in all conditions, but is extremely fast due to an efficient Simulink implementation.

The SCR catalyst model is based on a state space concept. The catalyst is discretized into six continually stirred tanks in the axial direction, and two wall layers are used to describe the mass transfer in the channel wall. Uniform radial flow and concentration distribution over the catalyst cross section is assumed; therefore it is sufficient to model one channel only. Eley-Rideal kinetics is applied to calculate the reaction rates on the catalyst surface. At low temperatures the model uses an implicit method of calculating the coverage differential. At higher temperatures, the model is simplified to a first order system using an operating condition dependent characteristic time constant. These simple, yet robust methods allow for long step lengths in the process of solving the differential equations. Using a 0.5 s time step, the computational performance is close to 100 times real time.

The engine-out NO_x, gas exchange and SCR models can be combined to a complete diesel engine and SCR system model. The combined model can be used to study the effects of varying EGR rate, injection pressure, injection timing and urea injection on NO_x formation and overall fuel/urea consumption. The integration of the models needs more work. A common exhaust temperature model must be developed to fully study the interaction between the systems. Using measured gas exchange parameters, the engine-out NO_x model and the SCR catalyst model have been integrated with excellent results however.

9 Future work

First, a common exhaust temperature model must be developed to properly integrate the three models. Also, the gas exchange model must be tuned to the current version of the experimental engine. These two actions will make the combined model entirely predictive.

The engine model does not incorporate multiple injections in its current form. Such models should eventually be included to be able to study the influence on NO_x and exhaust temperature.

The next major step in the project involves model based optimization. Driving sequences representative for real life driving is to be identified. The optimization procedure involves optimizing the fuel/urea consumption during real life driving sequences subject to the constraint that emission legislation must be achieved during the ESC/ETC with the same calibration. Possibly, further simplifications must be made to the engine and SCR models to achieve a satisfactory optimization time.

10 References

1. S. Hausberger, M. Ivanisin and I. J. Riemarsma, "Modelling of transient influences on HDV emissions", SAE_NA Technical Papers 2001-01-076, 2001.
2. R. Egnell, "Transient emission predictions for diesel engines with quasi stationary models", The Swedish national road and transport research institute, VTI Notat 16A-2005, 2005.
3. Q. Jiang and J. H. Van Gerpen, "Prediction of Diesel Engine Particulate Emission During Transient Cycles", SAE Technical Papers 920466, 1992
4. R. Egnell, "Combustion Diagnostics by Means of a Multizone Heat Release Analysis and NO Calculation, SAE Technical Papers 981424, 1998.
5. R. Egnell, "On Zero-dimensional Modelling of Combustion and NO_x Formation in Diesel Engines", Doctoral Thesis, Division of Combustion Engines, Department of Heat and Power Engineering, Lund Institute of Technology, Lund, 2001.
6. J. B. Heywood, "Internal Combustion Engine Fundamentals", McGraw-Hill Series in Mechanical Engineering, 1988, pp. 679-680, 572-577, 907-910.
7. L. Eriksson, "Mean Value Models for Exhaust System Temperatures", SAE Technical Papers 2002-01-0374, 2002.
8. M. Andersson, C. Nöhre, B. Johansson and A. Hultqvist, "A Real Time NO_x Model for Conventional and Partially Premixed Diesel Combustion", SAE Technical Papers 2006-01-0195, 2006.
9. M. Andersson, "Fast NO_x Prediction in Diesel Engines", Licentiate Thesis, Division of Combustion Engines, Department of Energy Sciences, Lund Institute of Technology, 2006.
10. R. J. Kee, F. M. Rupley and J.A. Miller, "The Chemkin Thermodynamic Data Base", Sandia report, SAND87-8215B, 1990.
11. C. Ericson, "Mean value modeling of a poppet valve EGR-system", Master's thesis, Vehicular Systems, Department of Electrical Engineering, Linköping University, 2004.
12. B. Westerberg, "Transient modelling of a HC-SCR catalyst for diesel exhaust aftertreatment", Chemical Engineering Journal 92 (2003) 27-39.
13. C. Ciardelli, I. Nova, E. Tronconi et. al. "SCR-DeNO_x for diesel engine exhaust aftertreatment: unsteady-state kinetic study and monolithic reactor modelling", Chemical Engineering Science 59 (2004) 5301-5309.
14. D. Murzin and T. Salmi, "Catalytic Kinetics", Elsevier, Amsterdam, 2005, pp. 285-288, 408.
15. L. Andersson, P. Gabrielsson and I. Odenbrand, "Reducing NO_x in Diesel Exhausts by SCR Technique: Experiments and Simulations", A.I.Ch.E. Journal 40 Issue 11 (1994) 1911-1919.
16. L. Andersson, "Mathematical Modelling in Catalytic Automotive Pollution Control", Doctoral Thesis, Department of Chemical Reaction Engineering, Chalmers University of Technology, 1995.

11 Summary of papers

Paper I

Transient emission predictions with quasi stationary models

C. Ericson, B. Westerberg and R. Egnell

SAE Technical papers 2005-01-3852, 2005

Quasi stationary calculations are applied to measurements from three diesel engines certified for Euro III. NO_x and fuel consumption is reasonably well predicted without any compensation. A transient correction method termed the Delay Model is developed to make time resolved correction of HC and PM emissions. The delay model has a physical interpretation in the sense that it estimates a turbocharger delay time and a corresponding corrected air-fuel equivalence ratio during transient operation. The overall results are satisfactory for predicting on road emissions from heavy duty engine populations, but lacks in accuracy to be used for simulation and optimization purposes.

The Delay Model was developed by the authors. The measurements were performed by Anders Hedbom at AVL/MTC as a part of the COST 346 project.

Paper II

Modelling diesel engine combustion and NO_x formation for model based control and simulation of engine and exhaust aftertreatment system

C. Ericson, M. Andersson, R. Egnell and B. Westerberg

SAE Technical papers 2006-01-0687, 2006

A simple and extremely computationally efficient predictive heat release and NO_x formation model is developed. The model uses a zero dimensional two zone concept. The combustion and NO_x formation models involve tabulated data to simplify the calculations. A simple gas exchange model of the filling and emptying type is added which makes the model a complete engine simulation package. The accuracy is excellent, a 10.4 % mean relative error is noted over a series of steady state points, and accumulated NO_x emissions over the ETC is predicted with a 7.1 % relative error.

The model was originally developed by Rolf Egnell and improved by the main author. The measurements were performed by Mikael Persson at Scania Engine Development.

Correction: the pre exponential factor of equation 24 should read $1.5 \cdot 10^9$.

Paper III

A state-space simplified SCR catalyst model for real time applications

C. Ericson, I. Odenbrand and B. Westerberg

To be submitted to SAE 2007 Powertrain and Fluid Systems.

A model of a vanadium based SCR catalyst of typical heavy truck dimensions is developed. The basic model structure is a series of continually stirred tank reactors using discretized catalyst walls to describe the mass transport. The model uses a state space concept. At low temperatures, an implicit step length is used to calculate the ammonia coverage. At higher temperatures, the model is simplified to a first order system using an operating condition dependent characteristic time constant. Combining these two methods allows for longer time step lengths compared to

previous models. The result is a SCR catalyst model of previously unseen computational efficiency. Yet the model shows agreement with measurements on par with more complex models.

The model in its original form was developed by Björn Westerberg. The methods applied to allow long step lengths were developed by the main author. The measurements were performed by Björn Westerberg at Scania Engine Development.